

Towards a deterministic model of planetary formation. III. Mass distribution of short-period planets around stars of various masses

S. Ida

Tokyo Institute of Technology, Ookayama, Meguro-ku, Tokyo 152-8551, Japan

UCO/Lick Observatory, University of California, Santa Cruz, CA 95064

`ida@geo.titech.ac.jp`

and

D. N. C. Lin

UCO/Lick Observatory, University of California, Santa Cruz, CA 95064

`lin@ucolick.org`

ABSTRACT

The origin of a recently discovered close-in Neptune-mass planet around GJ436 poses a challenge to the current theories of planet formation. Based on the sequential accretion hypothesis and the standard theory of gap formation and orbital migration, we show that around M dwarf stars, close-in Neptune-mass ice-giant planets may be relatively common, while close-in Jupiter-mass gas-giant planets are relatively rare. The mass distribution of close-in planets generally has two peaks at about Neptune mass and Jupiter mass. The lower-mass peak takes the maximum frequency for M dwarfs. Around more massive solar-type stars (G dwarfs), the higher-mass peak is much more pronounced. These are because planets tend to undergo type II migration after fully accreting gas around G dwarfs while they tend to migrate faster than gas accretion around M stars. Close-in Neptune-mass planets may also exist around G dwarfs, though they tend to be mostly composed of silicates and iron cores and their frequency is expected to be much smaller than that of Neptune-mass planets around M dwarfs and that of gas giants around G dwarfs. We also show that the conditions for planets' migration due to their tidal interaction with the disk and the stellar-mass dependence in the disk-mass distribution can be calibrated by the mass distribution of short-period planets around host stars with various masses.

Subject headings: planetary systems: formation – solar system: formation – stars: statics

1. Introduction

In an attempt to place quantitative constraints on models of planet formation, we developed an algorithm to simulate the kinematic properties of gas giants formed in isolation (Ida & Lin 2004a, hereafter Paper I). This prescription is based on the sequential accretion model in which we assume that Jupiter-mass gas-giant planets formed through 1) grain condensation, 2) runaway planetesimal coagulation (Greenberg et al. 1978; Wetherill & Stewart 1989; Aarseth et al. 1993; Kokubo & Ida 1996), 3) oligarchic growth of protoplanetary embryos (Kokubo & Ida 1998, 2000), and 4) gas accretion onto solid cores (embryos) (Mizuno 1980; Bodenheimer & Pollack 1986; Pollack et al. 1996; Ikoma et al. 2000). Based on a distribution of 1) dust-disk masses (M_d) inferred from mm data (Beckwith & Sargent 1996), 2) a range (1-10 Myr) of disk depletion time scale (τ_{dep}) inferred from the observed decline in the IR (Haisch et al. 2001) and mm data (Wyatt et al. 2003), and 3) three different growth-termination criteria (Lin & Papaloizou 1993; Bryden et al. 1999), we simulated a distribution of protoplanetary masses. In addition, we considered the effect of post formation type-II orbital migration due to planet-disk interaction (Lin & Papaloizou 1985) which is an important process in relocating protoplanets away from their birth places. The last process has been invoked (Lin et al. 1996) to account for the origin of a population of Jupiter-mass short-period planets such as 51 Peg b (Mayor & Queloz 1995).

We compared the results of our simulation with the available data of extrasolar planets. We suggested that around solar-type stars, 1) there may be a deficit of intermediate-mass ($\sim 20 - 100M_{\oplus}$) and intermediate-period ($\sim 0.1 - 1\text{yr}$) in their mass-period distribution (Paper I), 2) the frequency of gas giant planets may be an increasing function of their host stars' metallicity $[\text{Fe}/\text{H}]_*$ (Ida & Lin 2004b, hereafter Paper II), and 3) a large fraction of the planets migrated to the proximity of their host stars may have perished (Paper I, II). The first conclusion results directly from the expectation that a) the growth of protoplanetary cores is limited by dynamical isolation in the inner regions of planetary systems and slow coagulation rate in the outer regions, b) even under the most favorable locations, $0.1 - 1$ Myr is needed for the formation of protoplanetary embryos (cores), anywhere in the disk, with masses $M_c \gtrsim M_{\oplus}$, c) cores with mass larger than $M_{c,\text{acc}} \sim \text{several } M_{\oplus}$ can undergo runaway gas accretion, and d) orbital migration occurs on a similar time scale (τ_{mig}) to gas depletion in the disk (τ_{dep}).

The model we have presented so far provides the first step in the construction of deterministic properties of planetary formation. Its simplistic assumptions must be re-examined in a wider context of protoplanetary environment. For example, planets are assumed to form independently and in isolation in the model. Dynamical isolation in this context means that there are no other major planets around the same host stars. Most importantly, post-formation dynamical interaction between the planets have not yet been considered. While these effects will be examined in a future investigation, we consider here the mass function of dynamically-isolated planets and its dependence on the mass of the host star.

On the observational side, most of the known planets are found around solar-type stars (G

dwarf stars) because the most successful radial velocity surveys have been conducted for these target stars which have cool and well defined atmospheric spectroscopic features. However, the search window is rapidly expanding to lower-mass stars as detection techniques are being refined in both radial velocity and transit searches. Figure 1 shows the distributions of semimajor axis (a) and mass ($M_p \sin i$) of discovered extrasolar planets around M, K, G, and F stars. The planets around subgiants are excluded, because the relation between stellar spectral-type and its mass is different from that for main sequence stars. The planets discovered by transit survey are also excluded, because the transit survey has different observational bias in planetary periods from that of doppler survey. Although much more planets have been discovered around G stars than around F and K stars, the detection probability (after correction of metallicity dependence) is similar among these stars (Fischer & Valenti 2005). However, the detection probability may be by order of magnitude lower around M stars. Since their signals are the most conspicuous, close-in planets are expected to be the first to be uncovered (Narayan *et al.* 2004). However, until recently, the only planets discovered around M stars are two Jupiter mass planets with moderate semimajor axis (0.13AU, 0.21AU) around Gliese 876. No Jupiter-mass close-in planets have been discovered around M stars.

Recently, a short-period (2.6 days) Neptune-mass ($21M_\oplus$) planet is found to be orbiting around an M-dwarf ($M_* = 0.4M_\odot$) GJ436 (Butler *et al.* 2004). With a mass between those of gas giants and the Earth, this finding signifies a transition in the quest to search for terrestrial planets. In the solar system, two ice giants, Uranus and Neptune, have masses in this range. These planets are primarily composed of icy cores with a modest gaseous envelope. In accordance with the core accretion scenario, e.g., (Wuchterl *et al.* 2000), the cores in the outer solar system take a long time to emerge and when they finally acquired $M_{c,acc}$, the solar nebula was already so severely depleted that they can only accreted a small amount of gaseous envelope (Hayashi *et al.* 1985). It is natural to extrapolate that GJ436b may also have attained $M_{c,acc}$ but failed to accrete much gas. The main challenge to such a scenario is to account for the origin of both its low mass and short period.

The period of the first extrasolar gas giant planet (51 Peg b) discovered (Mayor & Queloz 1995) around a main sequence star outside the solar system is comparable to that of GJ436b. That planet and dozens others like it are thought to have formed through sequential accretion beyond the ice boundary and migrated to their present locations (Lin *et al.* 1996) as a consequence of their tidal interaction with their nascent gaseous disks (Goldreich & Tremaine 1980; Lin & Papaloizou 1985). But, the much lower mass M_p of GJ436b implies that gas accretion onto it may have been greatly suppressed prior to, during, and after its migration.

Two other short-period Neptune-mass planets have been found around G dwarfs (a planet with 2.8 day period and $15M_\oplus$ mass around 55 Cnc and that with 9.6 day period and $14M_\oplus$ mass around HD 160691) (McArthur *et al.* 2004; Santos *et al.* 2004). Since 55Cnc and HD160691 have three and two other giant planets (maybe gas giants), these Neptune-mass planets could form *in situ* by accumulation of rocky materials caused by sweeping mean motion resonance associated with migration of a giant planet, e.g., (Malhotra 1993; Ida *et al.* 2000) or sweeping secular resonance

associated with disk gas depletion, e.g., (Ward 1981; Nagasawa et al. 2000; Lin et al. 2004). Since we do not include interaction from other major planets, formation of these Neptune-mass planets is beyond scope of the present paper. On the other hand, no gas giant planets has been found around GJ436. GJ436b is dynamically-isolated, so that its formation must be considered without help of other giant planet(s) and our calculation in the present paper can address its formation.

Although in the present paper, we will propose a scenario that type II migration of a Neptune-mass planet occurs without significant gas accretion onto the planet around an M star, there are several other potential scenarios for the origins of dynamically-isolated, close-in Neptune-mass planets. Boss et al. (2002) suggested that, along with Jupiter and Saturn, Uranus and Neptune were formed through gravitational instability, in a massive disk. Heavy elements settled to form the cores and the gas envelope (clump) was greatly depleted by the photo-evaporation due to the UV flux from nearby OB stars before it contracts to planetary size. Since gravitational instability is unlikely at the present location (0.028AU) of GJ436b, the planet must have migrated from outer region by tidal interaction of the disk. However, the gravitational potential of disks around M stars is shallower than that around G stars such that the evaporation of the envelope of collapsing clumps would also eliminate all the residual gas in the disk. It would be difficult for the collapsing fragment to lose a large fraction of their mass and migrate extensively to form a GJ436b-like planet. On the other hand, under some extreme circumstance, the sporadic UV and X-ray irradiation from its host star could evaporate envelope of a gas giant planet that has migrated from outer region during M star’s main sequence lifetime. But the overall impact of the photoevaporation process on planet’s envelope and mass has not been determined.

Under the general concept of sequential accretion scenario, dynamically-isolated close-in planets may also form *in situ* (Bodenheimer et al. 2000). This scenario requires a concentration of planetesimals in the stellar proximity. One possible mechanism which may lead to such a situation is through embryo-disk interaction, or commonly known as type-I migration (Ward 1986, 1997a). The accumulation of building blocks for close-in planets also requires the termination of their migration process and the interaction between the embryos with their host stars as well as residual planetesimals.

Through a case study, we consider in this paper the origin of dynamically-isolated close-in planets of \sim Neptune mass around stars with various masses. With the model developed in Paper I and II, we show that Neptune-mass close-in planets may be abundant around M stars. In §2, we briefly recapitulate the sequential accretion hypothesis. Using our prescription, we first compare the mass function of dynamically-isolated close-in versus modest to long-period planets around solar-type stars (G dwarfs) in §3. This comparison is useful because we have most observational data and constraints for planets around solar-type stars at the present moment. Based on the best available observed properties of pre-main sequence evolutionary tracks of different-mass stars and accretion rates onto their host stars, we construct disk models around main sequence stars with various masses. In §4, we construct a conventional model of giant planet formation around lowest-mass stars and show that icy planets with $10\text{-}20M_{\oplus}$ accrete from planetesimals at $\sim 1\text{AU}$ without

any significant gas accretion onto the planets. These Neptune-mass planets can also readily migrate to the proximity of the stellar surface, where gas accretion is quenched at Neptune-mass. Through a series of simulations, we show, in §5, that the disk mass dependence on their host stars’ mass and the criteria of tidally induced migration in the disk may be quantitatively constrained by the mass distribution of short-period planets. We also place constraints, in §6, on the dependence of disk mass on the stellar mass. Finally, in §7, we summarize our results and discuss their implications.

2. Core accretion in disks around low-mass stars

The detailed description of sequential accretion scenario and our prescription to simulate the formation of planets are given in Paper I. We briefly recapitulate the central features of our approach and define various quantities which are used in the discussions of our results.

2.1. Growth of protoplanetary embryos

In the sequential accretion scenario, planetesimals grow into protoplanetary embryos (cores) which affects the velocity dispersion σ of nearby planetesimals and modifies their own growth (Ida & Makino 1993; Aarseth et al. 1993; Rafikov 2003). But, σ is also affected by gas drag (Kokubo & Ida 2002). In a disk with a surface density of dust (Σ_d) and gas (Σ_g) around a host star with mass M_* , protoplanetary embryos’ mass at any location a and time t is

$$M_c(t) \simeq \left(\frac{t}{0.48 \text{ Myr}} \right)^3 \left(\frac{\Sigma_d}{10 \text{ g cm}^{-2}} \right)^3 \left(\frac{\Sigma_g}{2.4 \times 10^3 \text{ g cm}^{-2}} \right)^{6/5} \left(\frac{m}{10^{22} \text{ g}} \right)^{-2/5} \left(\frac{a}{1 \text{ AU}} \right)^{-9/5} \left(\frac{M_*}{M_\odot} \right)^{1/2} M_\oplus, \quad (1)$$

where m is the typical mass of the planetesimals accreted by the embryos. Since accretion time $\tau_{c,\text{grow}} = M_c/\dot{M}_c$ increases with M_c , $M_c(t)$ does not depend on its initial value $M_{c,0}$ as long as $M_c(t) \gg M_{c,0}$.

In the limit of small σ , the full width of embryos’ feeding zone (Δa_c) is limited to $\sim 10r_H$ (Lissauer 1987; Kokubo & Ida 1998) where r_H is the embryos’ Hill’s radius $r_H (= (M_c/3M_*)^{1/3}a)$. When all the residual planetesimals in an embryo’s feeding zone have coagulated with it, the embryo attains an isolation mass

$$M_{c,\text{iso}} \simeq 0.16 \left(\frac{\Sigma_d}{10 \text{ g cm}^{-2}} \right)^{3/2} \left(\frac{a}{1 \text{ AU}} \right)^3 \left(\frac{\Delta a_c}{10r_H} \right)^{3/2} \left(\frac{M_*}{M_\odot} \right)^{-1/2} M_\oplus. \quad (2)$$

2.2. Protostellar disk properties

Equations (1) and (2) indicate that both $M_c(t)$ and $M_{c,\text{iso}}$ are determined by the distribution of Σ_d and Σ_g . In Paper I and II, we introduced a multiplicative factor (f_d and f_g) to globally scale

disks with the minimum mass nebula model for the solar system (Hayashi 1981) such that

$$\begin{cases} \Sigma_d &= 10\eta_{\text{ice}}f_d h_d (a/1\text{AU})^{-3/2} \text{ [g cm}^{-2}\text{]}, \\ \Sigma_g &= 2.4 \times 10^3 f_g h_g (a/1\text{AU})^{-3/2} \text{ [g cm}^{-2}\text{]}, \end{cases} \quad (3)$$

where the step function $\eta_{\text{ice}} = 1$ inside the ice boundary at a_{ice} and 4.2 for $a \geq a_{\text{ice}}$. [Note that the latter can be slightly smaller (~ 3.0) (Pollack et al. 1994).] The minimum mass model corresponds to $f_d = f_g \sim 1$. Here we introduced a new scaling factor, h_d and h_g , representing the dependence on stellar mass (see below).

If the disk is optically thin and heated by stellar irradiation only (Hayashi 1981),

$$a_{\text{ice}} = 2.7(L_*/L_\odot)^{1/2}\text{AU}. \quad (4)$$

The stars' luminosity L_* is generally a function of their mass M_* and age t . Additional heating due to viscous dissipation enlarges this boundary (Lin & Papaloizou 1980). This *ad hoc* phenomenological prescription provides a useful working hypothesis for comparative analysis between solar system architecture and extrasolar planetary systems. Since L_* is generally an increasing function of M_* , a_{ice} is small in disks around low-mass stars.

Around solar-type T Tauri stars, the observationally inferred total mass of dust, M_d , in the protostellar disks ranges from $10^{-5}M_\odot$ to $10^{-3}M_\odot$ (Beckwith & Sargent 1996), which corresponds to a range of $f_d \sim 0.1 - 10$. The disk-mass determinations are somewhat uncertain due to the poorly known radiative properties of the grains. Nevertheless, their divergent dust content provides a reasonable evidence for a greater than an orders of magnitude dispersion in M_d . In addition, the radio image of the disks is not well resolved in many cases. A rough magnitude of f_d can be inferred from the the total mass of the disk under the assumption that all disks have similar sizes (a few tens AU to a hundred AU). In this paper we follow Paper II and generate a set of f_d with a unit variant of Gaussian logarithmic distributions and a range between 0.1-10 with cut-off of high $f_d h_d$ tails at $30(M_*/M_\odot)$ (see Figure 4). If $f_g h_g \gtrsim 30(M_*/M_\odot)$, the disk is gravitationally unstable at $a \gtrsim$ a few AU (see discussion in section 7), and the total mass of heavy elements in the disk would be significant fraction of that in the host star.

In eq. (3), the dependence of Σ_d on M_* is incorporated in a mass scaling function h_d . In general, a relatively weak IR excess is associated with low-mass stars, which suggests h_d may be an increasing function of M_* , at least in the inner regions of the disk. For host stars with $M_* = M_\odot$, $h_d = 1$.

Equation (1) indicates that M_c is also a function of Σ_g through damping of σ due to gas drag. The planetary migration rate that we mention later is also dependent on Σ_g . Around other stars, very little information is available on Σ_g . Since there is no indication of divergent depletion pattern between molecular hydrogen and mm-size dust emission (Thi et al. 2001), we follow the same prescription for Σ_d with a disk mass scaling parameter f_g and a stellar-mass dependence function h_g (eq. [3]). Similar to Paper I and II, we adopt the conjecture that f_d does not change

except in those regions where they have been totally accreted by the cores and

$$f_g = f_{g,0} \exp\left(-\frac{t}{\tau_{\text{dep}}}\right), \quad (5)$$

where τ_{dep} is disk depletion time scale discussed below. The assumption of the uniform exponential decay is for simplicity. The effects of detailed decay pattern as a result of viscous evolution of disks will be discussed in a separate paper. For computational simplicity, we assume $[\text{Fe}/\text{H}]=0$, *i.e.*, a solar composition for all stars so that $f_d = f_{g,0}$ and $h_g = h_d$. The dependence of planetary $M_p - a$ distribution on $[\text{Fe}/\text{H}]$ for solar-type stars has already been discussed in Paper II.

We now consider a prescription for the stellar mass dependence. The parameters are h_d ($= h_g$) and τ_{dep} . In young clusters, the fraction of stars with detectable IR (Haisch et al. 2001) and mm continuum (Wyatt et al. 2003) from circumstellar disks around T Tauri stars declines on the time scales of 1-10 Myr. Although this decline may be due to dust growth and planetesimal formation rather than the depletion of heavy elements (D'Alessio et al. 2001; Tanaka et al. 2005), the correlation between the intensity of mm dust continuum with the gas decline emission (Thi et al. 2001) and the UV veiling for ongoing gas accretion suggest that gas is depleted as the dust signature fades. The dust signature maintains up to 10Myr also for disks around brown dwarfs (Mohanty et al. 2003). So, in this paper, we assume τ_{dep} in the range of 1-10 Myr for all stellar masses.

Although direct estimates of disk mass both in gas and dust are difficult to obtain for the inadequate sensitivity of existing observational instruments, the disk accretion rate \dot{M} can be inferred from the $\text{H}\alpha$ line profiles (Muzerolle et al. 2003; Natta et al. 2004) such that $\dot{M} \propto M_*^2$ with a large dispersion. If the angular momentum transfer and mass diffusion time scale is insensitive to M_* , we could infer h_g ($= h_d$) $\sim (M_*/M_\odot)^2$. In view of the large uncertainty in the data, we consider three possible dependence on M_* ,

$$h_d = (M_*/M_\odot)^{0,1,2}, \quad (6)$$

with $h_d = (M_*/M_\odot)^2$ as a standard case.

2.3. Core growth, isolation mass, and gas giant formation around stars with different masses

With these prescriptions for disk parameters, we find that

$$M_c(t) \simeq \left(\frac{t}{4.8 \times 10^5 \text{years}}\right)^3 \eta_{\text{ice}}^3 f_d^3 h_d^3 f_{g,0}^{6/5} h_g^{6/5} \left(\frac{a}{1\text{AU}}\right)^{-81/10} \left(\frac{M_*}{M_\odot}\right)^{1/2} M_\oplus, \quad (7)$$

by assuming $m = 10^{22}\text{g}$. From eq. (3), we estimate the core masses in protoplanetary systems with eq. (2) such that

$$M_{c,\text{iso}} \simeq 0.16 \eta_{\text{ice}}^{3/2} f_d^{3/2} h_d^{3/2} \left(\frac{a}{1\text{AU}}\right)^{3/4} \left(\frac{M_*}{M_\odot}\right)^{-1/2} M_\oplus. \quad (8)$$

We have already pointed out in Paper I and II that the growth of planetesimals is limited by isolation at small a and the slow coagulation rate at large a . Since for smaller M_* , r_H is larger, $M_{c,iso}$ is larger for the same mass disks. However, both h_d and h_g are increasing functions of M_* , so that the growth of $M_c(t)$ and the isolation mass $M_{c,iso}$ at any given a are actually smaller for lower-mass stars. We do not explicitly include type I migration (Ward 1986, 1997a) of cores, but take into account its effects in some runs (see Paper I and discussion in §5).

As the cores grow beyond a mass

$$M_{c,hydro} \simeq 10 \left(\frac{\dot{M}_c}{10^{-6} M_\oplus / \text{yr}} \right)^{0.25} M_\oplus, \quad (9)$$

their planetary atmosphere is no longer in hydrodynamic equilibrium and they begin to accrete gas (Stevenson 1982; Ikoma et al. 2000). In the above equation, we neglected the dependence on opacity (see Paper I). In regions where they have already attained isolation, the cores' accretion \dot{M}_c is much diminished and $M_{c,hydro}$ can be comparable to an Earth mass. But the gas accretion rate is still regulated by the efficiency of radiative transfer such that

$$\frac{dM_{p,g}}{dt} \simeq \frac{M_p}{\tau_{KH}} \quad (10)$$

where M_p is the planet mass including gas envelope and the Kelvin Helmholtz contraction time scale is (for details, see Paper II)

$$\tau_{KH} \simeq 10^{10} \left(\frac{M_p}{M_\oplus} \right)^{-3} \text{ yrs.} \quad (11)$$

Gas accretion onto the core is quenched when the disk is depleted either locally or globally. A protoplanet induces the opening of a gap when its rate of tidally induced angular momentum exchange with the disk exceeds that of the disk's intrinsic viscous transport (Lin & Papaloizou 1985), that is, when the planet mass M_p exceeds

$$M_{g,vis} \simeq \frac{40\nu}{a\Omega_K} M_* \simeq 40\alpha \left(\frac{h}{a} \right)^2 M_* \simeq 3 \left(\frac{\alpha}{10^{-4}} \right) \left(\frac{a}{1\text{AU}} \right)^{1/2} \left(\frac{L_*}{L_\odot} \right)^{1/4} M_\oplus, \quad (12)$$

where we used an equilibrium temperature in optically thin disks (Hayashi 1981) and α -prescription for the effective viscosity ν (Shakura & Sunyaev 1973), in which $T = 170(a/a_{ice})^{-1/2}$ K and $\nu = \alpha h^2 \Omega_K$ where α is a dimensionless parameter, h and Ω_K are the disk scale height and Kepler frequency. Since $h = c_s / \Omega_K$ where c_s is the sound velocity, $h^2 \propto T / M_* \propto L_*^{1/4} / M_*$, so that $M_{g,vis} \propto L_*^{1/4}$. Since L_* is an increasing function of M_* , eq. (12) indicates that $M_{g,vis}$ is smaller around lower-mass stars. The orbital evolution of planets is locked to the viscous evolution of the disk gas (type II migration) when their $M_p \geq M_{p,mig} = A_\nu M_{g,vis}$ where A_ν is the dimensionless factor $\sim 3 - 10$ for a laminar disk (Lin & Papaloizou 1985).

The type II migration rate \dot{a} is given by a/τ_{mig} with

$$\tau_{\text{mig}} = 10^6 f_g^{-1} h_g^{-1} \left(\frac{\alpha}{10^{-4}} \right) \left(\frac{M_p}{M_J} \right) \left(\frac{a}{1\text{AU}} \right)^{1/2} \text{ yrs}, \quad (13)$$

where M_J is Jupiter mass. We set a lower limit on τ_{mig} at $a^2/\nu \sim 4.3 \times 10^5 (\alpha/10^{-4})(a/1\text{AU})$ yrs (Paper I). We found that the formula for \dot{J}_m (angular momentum flux at the radius of maximum viscous couple, r_m) given in Paper I (eq. [63] in the paper) must be multiplied by a factor 2π . If we use \dot{J}_m to evaluate evolution of planetary orbital radius a , eq. (13) is reduced by 2π as well (Paper I). However, since the planetary migration may be caused by a fraction of \dot{J}_m and the fraction is uncertain, we use eq. (13) in the present paper too. We adjust the migration time scale by the value of α , which is also uncertain, comparing with observational data. As shown in Paper II, in order to reproduce period distribution of gas giant planets similar to that of observed extrasolar planets around solar-type stars, the disk viscous diffusion time scale $\tau_\nu = r_m^2/\nu \sim 4 \times 10^6 (\alpha/10^{-4})(r_m/10\text{AU})$ yrs must be comparable to disk lifetime τ_{dep} . Hence, the α viscosity in our model must be $\sim 10^{-4}$. Although the regions at 1-10AU could be "dead zone" for MHD turbulence (Sano et al. 2000), resulting in a very small α in these regions, the best fit value $\alpha \sim 10^{-4}$ may not necessarily reflect a realistic value because of rather simple assumptions for Σ_g distribution and its exponential decay in our model. We will carry out more detailed calculations coupled with disk viscous evolution in a separate paper.

The planets' migration is terminated either when the disk is severely depleted ($f_g \rightarrow 0$) or when they reach a_{stall} , which is set to be 0.04AU in our calculations. There are potential mechanisms to stop migration at $\lesssim 0.05\text{AU}$ (Lin et al. 1996). However, Paper II suggests that only a small fraction ($\lesssim 10\%$) of migrating planets can survive in the vicinity of their host stars. This fact should be kept in mind when population of close-in planets is discussed with our model.

The gap becomes locally severely depleted when the planets' Hill's radius (r_H) exceeds the disk thickness h (Bryden et al. 1999), that is, when M_p exceeds

$$M_{g,\text{th}} \simeq 120 \left(\frac{a}{1\text{AU}} \right)^{3/4} \left(\frac{L_*}{L_\odot} \right)^{3/8} \left(\frac{M_*}{M_\odot} \right)^{-1/2} M_\oplus. \quad (14)$$

Growth through gas accretion is quenched for planets with $M_p \geq M_{p,\text{trunc}} = A_{\text{th}} M_{g,\text{th}}$. Numerical simulations show some uncertainties in the dimensionless parameter A_{th} (Bryden et al. 1999; Nelson et al. 2000). Planets with $M_{p,\text{trunc}} > M_p > M_{p,\text{mig}}$ migrate with the disk while continue to accrete gas, albeit at a reduced rate, e.g., (Lubow et al. 1999). We use eq. (10) without a reduction factor for simplicity, because the reduction factor is quite uncertain and introduction of the factor does not affect the results significantly. Since gas accretion for $M_p > M_{p,\text{mig}}$ is already very rapid (11), the reduction does not change total gas accretion time scale. Following Paper I, we adopt in this paper $A_{\text{th}} = 1.5^3 \simeq 3.4$, that is, the truncation condition is $r_H > 1.5h$. Since L_* rapidly increases with M_* , $M_{p,\text{trunc}}$ is also smaller around lower-mass stars.

Even for planets with $M_p < M_{p,\text{trunc}}$, gas accretion may be ultimately limited by the diminishing amount of residual gas in the entire disk. For our disk models, the maximum available mass

is

$$M_{\text{g,noiso}} \sim \pi a^2 \Sigma_{\text{g}} \simeq 290 f_{\text{g},0} h_{\text{g}} \left(\frac{a}{1\text{AU}} \right)^{1/2} \exp \left(-\frac{t}{\tau_{\text{dep}}} \right) M_{\oplus}. \quad (15)$$

When $M_{\text{g,noiso}}$ becomes smaller than M_{p} , gas accretion is terminated.

A similar global limit $M_{\text{c,noiso}} = \pi a^2 \Sigma_{\text{d}}$ (see eq. [20]) is also imposed if the formula (2) exceeds it. As the gas is severely depleted, the velocity dispersion σ of the embryos and residual planetesimals grows until they cross each other's orbits (Iwasaki et al. 2002; Kominami & Ida 2002). Eventually a few surviving embryos acquire most of the residual planetesimals and less massive cores during the late oligarchic-growth stage. The asymptotic embryos' masses are given by eq. (2) with $\Delta a_{\text{c}} \sim V_{\text{surf}}/\Omega_{\text{K}}$,

$$M_{\text{e,iso}} \simeq 0.52 \eta_{\text{ice}}^{3/2} f_{\text{d}}^{3/2} h_{\text{d}}^{3/2} \left(\frac{a}{1\text{AU}} \right)^{3/2} \left(\frac{\rho_{\text{d}}}{1\text{gcm}^{-3}} \right)^{1/4} \left(\frac{M_{*}}{M_{\odot}} \right)^{-3/4} M_{\oplus} \quad (16)$$

where V_{surf} and ρ_{d} are the surface escape speed and internal density of the embryo. We use this enlarge asymptotic mass when $f_{\text{g}} < 10^{-3}$.

In Paper I and II, we put all of these processes into a numerical scheme to simulate the formation and migration probabilities of planets around solar-type stars. Cores with $M_{\text{p}} > M_{\text{c,acc}}$ emerge on time scale shorter than τ_{dep} in disks with modest-to-large values of f_{d} around solar-type stars. In this limit, gas accretion and orbital migration lead to the formation of gas giants with kinematic properties similar to those observed.

3. Emergence and migration of Neptune-mass planets in disks around solar-type stars

We now apply our numerical methods to study the formation of planets around stars with various masses. Our objective is to simulate the mass function of close-in planets and assess the influence of formation and migration on it. We show here that this quantity can provide clues on the dominant processes which regulate planet formation and it also can be used to distinguish between competing theories of planet formation. In all models, we choose $\alpha = 10^{-4}$ based on assumption that the viscous evolution time scale for the disks is comparable to τ_{dep} (see §2.3). Using these models, we carry out Monte Carlo simulations. For simplicity, we generate a set of initial a 's of the protoplanets and τ_{dep} with uniform distributions in log scale in the ranges of 0.1–100AU and 10^6 – 10^7 yrs. The assumed a distribution corresponds to orbital separations Δa that is proportional to a , which may be the simplest choice. The distribution of f_{d} was discussed in §2.2 (also see Figure 4). In Paper I and II, we also assumed a distribution of M_{*} in a range of 0.7–1.4 M_{\odot} . In this paper, in order to make the M_{*} dependence clear, the value of M_{*} is fixed in each run.

In the following sections, we consider several sets of model parameters. We first discuss a standard model with $A_{\nu} = 10$ and $h_{\text{d}} = (M_{*}/M_{\odot})^2$ around a solar-type star with $M_{*} = 1.0M_{\odot}$ (model 1.0). The evolution of totally 20,000 planets are calculated for each run.

3.1. Formation of cores and asymptotic mass of protoplanets.

Model 1.0 is similar to the results we have already presented in Paper I. In Figure 2a, we highlight the mass ($M_{\text{p,fin}}$) and semi major axis (a_{fin}) distribution of planets at $t = 10^9$ yrs after they have attained their asymptotic mass and gone through the initial migration due to their tidal interaction with their nascent disks. The main features to notice in this panel are: 1) a deficit of planets with intermediate masses ($20 - 100M_{\oplus}$) at intermediate semi major axis ($0.1 - 1\text{AU}$), and 2) a large population of close-in ($a_{\text{fin}} < 0.05\text{AU}$) gas giants with $20M_{\oplus} \lesssim M_{\text{p}} \lesssim 2 \times 10^3 M_{\oplus}$, although only a small fraction of them ($\lesssim 10\%$) may be able to survive (Paper II). We have already indicated in Paper I that these properties are due to 1) the runaway nature of dynamical gas accretion and 2) type II migration.

In order to distinguish between these two dominant effects, we trace back, in Figure 2b, the initial semi major axis (a_{ini}) where the cores of both close-in (marked by black circles) and intermediate or long-period planets (marked by gray dots) formed. These results clearly indicate an one-to-one mapping between the mass function of the close-in planets and the locations where they are formed. For illustrative purposes, we also mark the domain where some physical processes operate and dominate the evolution of protoplanets. For example, the thin solid lines indicate the upper limit of the isolation mass that cores can attain prior to gas depletion (it is obtained with $f_{\text{d}} = 30$ in $M_{\text{c,iso}}$ and $M_{\text{c,noinso}}$). The transition at 2.7 AU in model 1.0 corresponds to the ice boundary. The thick solid lines indicate the critical mass for the onset of type II migration, $M_{\text{p,mig}} = A_{\nu} M_{\text{g,vis}}$ with $A_{\nu} = 10$ according to eq. (12). We also highlighted the asymptotic growth limit $M_{\text{p,trunc}} = A_{\text{th}} M_{\text{g,th}}$ with $A_{\text{th}} = 3.4$ (eq. 14) by broken lines.

At any given a_{ini} , a fraction of terrestrial planets can form with M_{p} above $M_{\text{p,iso}}$ through 1) gas accretion and 2) merger of residual planetesimals and other embryos after disk gas depletion. When the embryos reach their isolation mass, $M_{\text{c,hydro}}$ declines with the vanishing \dot{M}_{c} (eq. [9]). Although gas accretion is initiated, planets cannot grow significantly prior to severe gas depletion unless the planets' isolation mass $M_{\text{c,iso}} \gtrsim M_{\text{c,acc}} \simeq \text{several } M_{\oplus}$. The gas accretion time scale given by eq. (11) can be comparable to or shorter than τ_{dep} only for cores with $M_{\text{c}} \gtrsim \text{several } M_{\oplus}$. Mergers of residual planetesimals and other embryos occur during and after the gas depletion (see eq. [16] for asymptotic $M_{\text{c}} \sim M_{\text{e,iso}}$) (Kominami & Ida 2002).

If their $M_{\text{p}} > M_{\text{p,mig}} = A_{\nu} M_{\text{g,vis}}$ and there is adequate residual gas in the disk (f_{g} is still large enough), they would migrate to the vicinity of their host stars (eq. [13] with eq. [5]). The magnitude of $M_{\text{g,vis}}$ is an increasing function of a . For $a \lesssim 0.7 \text{ AU}$, τ_{KH} for embryos which can migrate is longer than their τ_{mig} . Although their M_{p} may be $< M_{\text{p,trunc}} = A_{\text{th}} M_{\text{g,th}}$, their inward migration is sufficiently rapid that they do not acquire a significant amount of gas along the way (Ivanov et al. 1999). Termination of migration allows low-mass planets (formed at $a \lesssim 0.7\text{AU}$ in relatively massive disks) to grow through gas accretion to their asymptotic mass $M_{\text{p,trunc}} \simeq 30M_{\oplus}$ at the stalling location which is set to be $a_{\text{stall}} = 0.04 \text{ AU}$. Thus, the final mass of close-in planets with $a_{\text{ini}} \lesssim 0.7\text{AU}$ is $\simeq 30M_{\oplus}$ regardless of truncation mass $M_{\text{p,trunc}}$ at the original locations a_{ini} .

These planets are formed interior to the ice boundary and they are likely to be mostly composed of silicates and iron, in contrast to the ice giants in the solar system. Also, they cannot accrete large amount of gas because the aspect ratio of their nascent disk at 0.04 AU is so small that they induce clear gap formation when their mass reaches that of Neptune.

Planets formed at slightly larger a 's ($\sim 1\text{AU}$) must attain $M_p \gtrsim 20 - 30M_\oplus$ before they acquire the mass to start migration, $M_{p,\text{mig}} = 10M_{g,\text{vis}}$ (eq. [12]). With this critical mass, embryos which can initiate migration there can also accrete gas efficiently with $\tau_{\text{KH}} < \tau_{\text{mig}}$ provided the gas in the disk is not severely depleted. Since $M_{p,\text{trunc}}$ decreases with decrease in a , when they arrive close to their host stars, their M_p may be $> M_{p,\text{trunc}}$ so that they would not acquire any additional mass. Note that cores of these planets are also mostly made of silicates and iron rather than ice and they should not be referred to as hot Neptunes.

At even larger radius, $M_{c,\text{iso}} \gtrsim 5 - 10M_\oplus$. Prior to reaching isolation, embryos' gas accretion is suppressed by the bombardment of residual planetesimals, *i.e.*, $M_c < M_{c,\text{hydro}}$ for moderate \dot{M}_c . After isolation is reached, $M_{c,\text{hydro}}$ becomes smaller than M_c and their τ_{KH} due to gas accretion is reduced below τ_{mig} and they quickly evolve into gas giants. Thus, final M_p in Figure 2b coincides with $M_{p,\text{trunc}}$ at initial locations. Beyond $\sim 10\text{ AU}$, the time scale for the emergence of cores with $M_p > M_{c,\text{acc}}$ or isolation is comparable to or longer than both τ_{mig} or τ_{dep} . Although they may acquire M_p in the range of $10 - 100M_\oplus$ through merges of residual embryos after the gas depletion, these planets generally do not migrate extensively.

3.2. Mass distribution of short-period planets

Interior to the ice boundary, nearly all the planets with sufficient mass to initiate efficient gas accretion have migrated to the vicinity of the host star (see Figure 2b). But, a majority of the planets which migrated to the vicinity of solar-type stars were formed beyond the ice boundary, as gas giants, prior to their migration. There is a narrow window in the range of a where the seed of intermediate-mass planets may form and migrate to the proximity of their host stars. In Figure 3, theoretically predicted mass distributions are plotted. Since it is expected that most of close-in planets may fall onto their host stars, we plot the distributions of close-in planets, reducing the amplitude N by a factor 10. For comparison of the amplitude between close-in and distant planets, uncertainty in this calibration is noted. We also plotted observed distributions. Since the number of runs in each model does not reflect the number of targets for current doppler survey, we cannot compare the amplitude N between the observed and the theoretically predicted distributions. Only the shape of the distributions should be compared. Also note that observed distributions do not exactly correspond to host stars' mass of each model and numbers of observed planets are not large enough for statistical arguments for stars other than G stars (model 1.0). We show that, around stars with $M_* \simeq 1M_\odot$, the mass distribution for the close-in (with $a_{\text{fin}} < 0.05\text{ AU}$) planets is skewed toward $\sim 10^3M_\oplus$ (model 1.0 in Figure 3a). This distribution is more enhanced near $\sim 10^3M_\oplus$ than that observed. The effect of post formation star-planet tidal interaction, which has not been taken

into account in our model, may have caused the demise of a majority of the close-in planets, in particular massive planets (Gu *et al.* 2003, Paper II).

In disks with modest masses, planets form in the advance stages of evolution when gas depletion is well underway. Some of these planets may migrate interior to the ice boundary and become stalled while others remain close to their place of birth. A majority of gas giant planets with $0.1\text{AU} \lesssim a_{\text{fin}} \lesssim 1\text{ AU}$ have migrated but not extensively. In contrast to the close-in planets, model 1.0 in Figure 3b clearly shows a paucity of longer-period ($0.1\text{AU} \lesssim a_{\text{fin}} \lesssim 1\text{ AU}$) planets at $M_{\text{p}} \sim 20 - 100M_{\oplus}$. This distribution reflects the stringent prerequisite that gas accretion into gas giants must be preceded by the rapid formation of sufficient mass cores whereas the build up of terrestrial planets can continue well after the severe depletion of the disk.

4. Dependence on the stellar mass

In a generalization of the solar nebula model, Nakano (1988) showed that the temperature distribution throughout the disk increases with M_* . However, he did not consider the dependence of Σ_{d} and Σ_{g} on M_* . In a recent paper, Laughlin, Bodenheimer & Adams (2004), considered a model in which the disk mass increases with the stellar mass. Their objective is to demonstrate the difficulties to form gas giants around M dwarf stars. But, the effects of planetary migration, truncation of gas accretion due to gap opening and the gradual depletion of the disk gas are neglected.

In this section, we consider the variation of 3 model parameters: 1) the stellar mass M_* , 2) the dependence of disk mass on the stellar masses, h_{d} , and 3) the condition for the onset of type II migration. A standard series are Model x where $x = 0.2, 0.4, 0.6, 1.0, 1.5$ represents models with $M_* = xM_{\odot}$. In the standard series, we set $A_{\nu} = 10$ and $h_{\text{d}} = (M_*/M_{\odot})^2$. Model xB (series B) and xC (series C) correspond to $A_{\nu} = 1$ and 100 with $h_{\text{d}} = (M_*/M_{\odot})^2$. x in xB and xC expresses M_*/M_{\odot} as well. Model xD (series D) and xE (series E) correspond to $h_{\text{d}} = M_*/M_{\odot}$ and 1 with $A_{\nu} = 10$.

In Figure 4, distributions of $f_{\text{d}}h_{\text{d}}$ we used for models x and xB are shown. They represent the relative mass distribution of disks around stars with various masses. The mean value of Σ_{d} is an increasing function of M_* (see eq. [3]). In order to limit additional model parameters, we assume ZAMS mass-luminosity relationship, $L_*/L_{\odot} = (M_*/M_{\odot})^4$. Since the time scale of pre-main sequence stage of lower-mass stars is long, planet formation around these stars may proceed during their pre-main sequence stage in which L_* is rather large. In that case, the dependence of L_* on M_* is weaker, but it may still have a positive power-law dependence, so that the trend of the M_* -dependence of planetary systems shown below does not change.

In the calculations in this section,

$$a_{\text{ice}} = 2.7 \left(\frac{M_*}{M_{\odot}} \right)^2 \text{ AU}, \quad (17)$$

$$M_p(t) = \left(\frac{t}{4.8 \times 10^5 \text{years}} \right)^3 \eta_{\text{ice}}^3 f_d^{21/5} h_g^{6/5} \left(\frac{a}{1\text{AU}} \right)^{-81/10} \left(\frac{M_*}{M_\odot} \right)^{89/10} M_\oplus, \quad (18)$$

$$M_{\text{c,iso}} = 0.16 \eta_{\text{ice}}^{3/2} f_d^{3/2} \left(\frac{a}{1\text{AU}} \right)^{3/4} \left(\frac{M_*}{M_\odot} \right)^{5/2} M_\oplus, \quad (19)$$

$$M_{\text{c,noiso}} \simeq 1.2 \eta_{\text{ice}} f_d \left(\frac{a}{1\text{AU}} \right)^{1/2} \left(\frac{M_*}{M_\odot} \right)^2 M_\oplus, \quad (20)$$

$$M_{\text{e,iso}} = 0.52 \eta_{\text{ice}}^{3/2} f_d^{3/2} \left(\frac{a}{1\text{AU}} \right)^{3/2} \left(\frac{\rho_d}{1\text{gcm}^{-3}} \right)^{1/4} \left(\frac{M_*}{M_\odot} \right)^{9/4} M_\oplus, \quad (21)$$

$$M_{\text{p,mig}} = A_\nu M_{\text{g,vis}} = 30 \left(\frac{A_\nu}{10} \right) \left(\frac{\alpha}{10^{-4}} \right) \left(\frac{a}{1\text{AU}} \right)^{1/2} \left(\frac{M_*}{M_\odot} \right) M_\oplus, \quad (22)$$

and

$$M_{\text{p,trunc}} = A_{\text{th}} M_{\text{g,th}} = 400 \left(\frac{A_{\text{th}}}{1.5^3} \right) \left(\frac{a}{1\text{AU}} \right)^{3/4} \left(\frac{M_*}{M_\odot} \right) M_\oplus. \quad (23)$$

4.1. Planets around M dwarf stars

In Figures 2 and 3, we also included the results of the simulations for models 0.2-0.6 and 1.5. We first present a low-mass model 0.2 since it is in strong contrast to model 1.0. Stars with $M_* = 0.2M_\odot$ corresponds to relatively light M stars. These stars are not only most numerous but they also contribute most to the initial stellar mass function. According to our prescription and model parameters, Σ_g and Σ_d around the host star in model 0.2 are 25 times smaller than those in model 1.0.

In the result of model 0.2 on the top panels of Figures 2a and b, we find that Jupiter-mass planets rarely formed around low-mass stars. This paucity is due to the slow growth rate of embryos and their low isolation mass such that little gas can be attained by them prior to its depletion. This result confirms the conclusion reached earlier by Laughlin, Bodenheimer & Adams (2004).

The upper limit of the $M_{\text{p,fin}} - a_{\text{fin}}$ distribution is determined by the $M_{\text{c,iso}}$. This correlation arises because L_* is a rapidly rising function of M_* . In our prescription, the ice boundary is located at $a_{\text{ice}} \simeq 0.11\text{AU}$ (eq. [17]) which is 25 times closer to a host star with $M_* = 0.2M_\odot$ than in model 1.0 with solar-type stars. Nearly all the cores formed around these low-mass stars are mostly composed of ice. Planets can acquire masses $M_p > M_{\text{c,iso}}$ through gas accretion. But with a relatively small $M_{\text{c,iso}}$, the accretion is inefficient (eq. [11]). They can also gain mass after the gas depletion through collisions and mergers of residual embryos. But the asymptotic mass $M_{\text{e,iso}}$ is also relatively small for low-mass stars (eq. [21]).

With the *ad hoc* α prescription we have adopted, the necessary condition for the onset of type II migration is satisfied for relatively low-mass planets (eq. [22]). When their $M_p > M_{\text{p,mig}}$, these cores undergo orbital decay. Similar to model 1.0, there is a population of close-in planets with

$2M_{\oplus} \lesssim M_p \lesssim 10M_{\oplus}$. The results on the top panel of Figure 2b show that they indeed originated from a region between a_{ice} and ~ 3 AU. They also indicate that planets with mass down to $2M_{\oplus}$ may migrate to the proximity of a $0.2M_{\odot}$ star. At the arbitrary $a_{\text{stall}} = 0.04$ AU around such a host star, the equilibrium temperature of these close-in Neptune-mass planets is similar to that of the Earth. The composition and structure of such planets have been already been discussed by Léger et al. (2004).

Although a few planets formed with $M_p > 10M_{\oplus}$, they are the exceptional cases resulting from the tails of the f_d distribution. Consequently, the mass function of planets with modest or large $a_{\text{fin}} (> 0.1$ AU) show a sharp decline at $M_p \sim 10M_{\oplus}$ (Figure 3b). It also extends well into the low-mass range. In contrast, the mass function for the close-in planets (with $a_{\text{fin}} < 0.05$ AU) shows a peak near $M_p \sim 10M_{\oplus}$ (Figure 3a).

In model 0.4, we consider a host star with $M_* = 0.4M_{\odot}$ which corresponds to a relatively massive M dwarf star. It is an analog of GJ436, around which a single close-in Neptune-mass planet has been discovered (Butler et al. 2004). Figure 3a and b indicate that the frequency of planets observable with current doppler survey is significantly smaller for M stars than for K, G, and F stars (also see Figure 8). This is consistent with the observation and the finding of Laughlin, Bodenheimer & Adams (2004).

Figure 5 indicates the mean mass and characteristic mass associated with the highest peak of the mass distribution for a) the close-in planets and b) planets with $0.1 < a < 1$ AU. These masses increase with M_* , in particular for the close-in planets. This accounts for the recent planetary finding around GJ436.

We find *the frequency of Neptune-mass close-in planet peaks at $M_* \sim 0.4M_{\odot}$* (Figures 3a and 5). The formation of these planets depends sensitively on the environment and their frequency provides constraints on the sequential accretion scenario. Most of these planets formed slightly beyond the ice boundary. For this stellar mass, the ice boundary is located at $\simeq 0.43$ AU. Outside it, the upper limit of $M_{\text{c,iso}}$ exceeds $M_{\text{p,mig}}$. In Figure 6, we illustrate the evolution of a typical embryo that forms near the ice boundary in a disk with $h_d f_d = 7.2$ and a depletion time scale $\tau_{\text{dep}} = 9.2$ Myr. The disk surface density $h_d f_d = 7.2$ is close to the tail of the distribution for $0.4M_{\odot}$ stars (Figure 4). During the initial 2×10^4 yrs, an embryo grows to $\sim 10M_{\oplus}$ through coagulation. The rapid coagulation enhances $M_{\text{c,hydro}}$, which prevents gas accretion (see eq. [9] and Figure 6). Since this embryo is located beyond the ice boundary and $h_d f_d = 7.2$, $M_{\text{c,iso}}$ is as large as $\simeq 30M_{\oplus}$. But, before it acquires $M_{\text{c,iso}}$, it opens up a gap and undergoes type II migration at $M_c \sim 10M_{\oplus}$. During the migration, gravitational perturbations from the embryo prevents additional planetesimals from reaching the embryo and its growth is quenched (Tanaka & Ida 1997; Rafikov 2003). On a time scale of 3×10^5 yr, the embryo migrates to 0.04 AU where it is stalled. The termination of bombardment by residual planetesimals makes $M_{\text{c,hydro}}$ lower to start gas accretion onto the embryo. However, the gas accretion time scale τ_{KH} is longer than τ_{mig} (Figure 4). Gas accretion onto the planet actually proceeds after it reaches 0.04AU. The planet's

growth is quenched at $\simeq 14M_{\oplus}$ as a clean gap is formed because $M_{p,\text{trunc}} \simeq 14M_{\oplus}$ at 0.04AU. Figures 2 and 3 show that many planets evolve in a similar way to acquire $M_{p,\text{fin}} \simeq 14M_{\oplus}$. The composition of these planets is similar to that of Uranus and Neptune and its day-side surface temperature may be $\sim 500\text{K}$.

In the lowest-mass model 0.2, the upper limit of $M_{c,\text{iso}}$ does not exceed $M_{p,\text{mig}}$ even outside the ice boundary. The migration of Neptune-mass planets requires a delicate balance between $M_{c,\text{iso}}$ and $M_{p,\text{mig}}$. Thus, the frequency of close-in Neptune-mass planets in model 0.4 is larger than that in model 0.2.

This frequency in model 0.4 is also larger than that in model 1.0. Although the upper limit of $M_{c,\text{iso}}$ is larger than $M_{p,\text{mig}}$ outside the ice boundary around solar-type stars, $M_p \gtrsim 30 - 40M_{\oplus}$ at the onset of migration, so that gas accretion is much more efficient onto such large cores (eq. [11]). Thus, most isolated planets tend to arrive at the proximity of a solar-type star as gas giants and only a small fraction arrives as silicate and iron cores with limited gaseous envelopes.

Recently Neptune-mass planets have been detected around 55Cnc and HD160691 (McArthur et al. 2004; Santos et al. 2004). Since these stars are G-type stars, if the result of Figure 3 is applied, the probability of formation of such planets is very low although it is not zero. Unlike GJ436, there are three additional Jupiter-mass planets around 55Cnc and two additional ones around HD160691. In the system of 55Cnc, sweeping mean motion resonance associated with migration of the giant planet (Malhotra 1993; Ida et al. 2000) presently at 0.1AU could bring rocky embryos/planetesimals to the vicinity of the host star, so that a Neptune-mass rocky planet could accrete *in situ*. On the other hand, in the system HD160691, sweeping secular resonance associated with disk gas depletion (Ward 1981; Nagasawa et al. 2000), could bring rocky embryos/planetesimals to inner regions (Lin et al. 2004). In the present paper, we do not include such interactions. We will present elsewhere details. In the system of GJ436, however, no additional Jupiter-mass planet has been found. Our model accounts for formation of the isolated Neptune-mass planet around an M star.

4.2. Planets around K dwarfs

Figure 3b shows that in model 0.6 where $M_* = 0.6M_{\odot}$, the intermediate-mass ($20 - 100M_{\oplus}$) and intermediate-*a* (0.1 – 1AU) planets are more abundant than in either model 1.0 or model 0.4. The mass function of close-in planets also appears to be smoother with some M_p in the range of $\sim 10 - 100M_{\oplus}$ (Figure 3a). These intermediate-mass planets formed just outside the ice boundary in disks with modest f_d where the upper limit of $M_{c,\text{iso}} \sim 50 - 100M_{\oplus}$ while that for typical disks (with $f_d \sim 1$) is $\sim M_{\oplus}$. The critical mass for starting planetary migration at the ice boundary is $20M_{\oplus}$ in model 0.6. A small fraction of emerged cores may accrete modest amount of gas as it starts to migrate.

The formation of the intermediate-mass and intermediate-*a* planets, which tends to smooth the mass distribution, may be one of characteristics of planets around K stars, compared with

those around G and F stars, although it is much less pronounced than the characteristics of planets around M stars. For illustration, we present, in Figure 7, the formation of a typical planet which formed with an intermediate mass and attain an intermediate a during its migration. In this case, a seed embryo is formed at $a_{\text{ini}} = 1.8\text{AU}$ in a slightly massive $h_d f_d = 2$ disk with $\tau_{\text{dep}} = 2.3\text{Myr}$. Through planetesimal coagulation, this embryo attains a mass $M_p \simeq 8M_\oplus$ and become isolated in 1.5 Myr. The cessation of the planetesimal bombardment enables the embryo to grow through gas accretion. When its mass reaches $M_p = 30M_\oplus$ at $\sim 8\text{ Myr}$, gas accretion is quenched by the severe depletion of gas near its orbit. The newly formed planet undergoes migration while gas is globally depleted. The orbital migration is eventually halted at an intermediate location, 0.4AU.

The condition for growth to be quenched between $10 - 100M_\oplus$ requires $a \sim 1\text{ AU}$. The above example shows that to halt migration at an intermediate location, both time scales of migration and growth due to gas accretion are required to be comparable to the gas depletion time scale. In general, such special circumstances are satisfied with small probability. However, they are more likely around K dwarfs than other type stars because cores with $M_p \gtrsim 10M_\oplus$ are more abundant at $a \sim 1\text{AU}$ around K dwarfs as a result of the M_* dependence of a_{ice} and $M_{\text{c,ico}}$. In model 0.6, gas accretion may be quenched when the cores attain a mass $10M_\oplus \lesssim M_p \lesssim 100M_\oplus$ while they migrated to $0.04\text{AU} \lesssim a \lesssim 1\text{ AU}$. In comparison with model 1.0, the isolation mass $M_{\text{c,iso}}$ at the ice boundary increases with M_* . Around a solar-type star, the isolation mass near the ice boundary is sufficiently large for efficient gas accretion to be initiated. Eventually runaway gas accretion leads to the emergence of the intermediate-mass deficit in the mass distribution of planets around relatively high-mass stars. Figure 1 shows that some fraction of planets discovered around K stars may have the intermediate mass. However, the number of the detected planets may be insufficient for statistical discussion. These stellar mass dependence in the extrapolated planetary characteristics can be tested with future observation.

4.3. Planets around higher-mass stars

In model 1.5 where $M_* = 1.5M_\odot$, the range of a where gas giants are formed is more extended (the bottom panel in Figures 2). This arises primarily because the disks around more massive stars have relatively large Σ_d . In this case, $M_{\text{c,acc}}$ (the core mass required for rapid gas accretion) can be attained before gas depletion even at large a . However, larger a_{ice} in this case leads to slow core growth beyond the ice boundary. Thus, most gas giants have cores composed of silicates and iron but not icy cores, in contrast with gas giants around lower mass stars. The very large a_{ice} also leads to less efficiency of formation of gas giants in the range of a few AU to 10AU than that around G stars, although gas giants form in broader range of a . As a result, the fraction of F stars harboring giant planets with periods smaller than several years which are currently detectable with doppler survey is rather smaller than that of G stars (Figure 8), although the difference is within a factor 1.5. The similar fraction within a factor 2 among K, G, and F stars shown in Figure 8 is consistent with the observation (Fischer & Valenti 2005). The predicted mass distributions for M, K, G, and

F stars are not inconsistent with the observed distributions. Since the numbers of observed planets are not enough for statistical discussion, in particular for stars other than G stars (Figure 3), we cannot discuss the agreement between the predicted and observed distributions in more detail.

Strong winds and jets from further higher mass stars (A, B stars) may decrease τ_{dep} , which reduces formation rate of gas giants. It is not clear how much the fraction of massive stars with gas giant planets is reduced. We will address planetary formation around massive stars elsewhere.

5. Dependence on the migration condition

The results of the standard models clearly indicate that the mass function of planets depends on the delicate balance between growth and migration time scales. There are some uncertainties concerning the migration process. In the standard series, we set $A_\nu = 10$ (eq. [22]) in accordance with the results of previous numerical simulations (Lin & Papaloizou 1985). However, the additional contribution from a torque imbalance between the Lindblad resonances of low-mass embedded cores may also lead to type I migration while their masses are relatively small (Goldreich & Tremaine 1980; Ward 1986, 1997a), although turbulence in the disk (Nelson & Papaloizou 2004; Laughlin, Steinacker & Adams 2004) and self induced secondary instability (Balmforth & Korycansky 2001; Koller et al. 2003) can also retard the rate of migration. In our simulations, we can partly take into account the effect of type I migration by lowering the value of A_ν (to unity). We also carried out simulations with $A_\nu (= 100)$ such that the onset of migration is delayed until the cores have attained relatively large masses.

The sensitive dependence of the mass function of close-in planets on the migration condition makes it an ideal observable feature which can be used to calibrate the criteria and efficiency of migration. In a variation of the standard models, we consider two new series: 1) series B (model *x*B) with $A_\nu = 1$ and 2) series C (model *x*C) with $A_\nu = 100$, which have identical M_* as the standard series with $A_\nu = 10$. In Figures 9a and b, we show the final mass and semimajor axis distribution of planets in models *x*B and *x*C.

For models *x*B, cores undergo migration before they attain sufficient mass to engage in efficient gas accretion. Although the cores' migration may terminate close to their host stars, the relatively small aspect ratio of the disk for small a implies low $M_{\text{p, trunc}}$. At small a , gap formation prevents the cores from accreting gas. The accumulation of cores and planetesimals in the proximity of their host star may promote their coagulation (Ward 1997b). Although we cannot rule out the possibility of a highly-efficient migration on the basis of the mass function of the close-in planets, it does pose difficulties to account for the modest frequency of gas giants with periods longer than a few weeks. Even around solar-type stars, cores rapidly migrate to the stellar proximity before they have acquired sufficient mass to efficiently accrete gas so that the probability of gas-giant formation is strongly suppressed.

For the low-stellar-mass models 0.2B and 0.4B, the isolation mass is only a few times larger than

that of the Earth. Nevertheless, it is larger than $M_{\text{p,mig}}$ for this low- A_ν case. Most cores migrate toward their host stars with M_{p} less than a few M_\oplus . Although these masses are $< M_{\text{p,trunc}}$, gas accretion is too slow (eq. [11]) for them to acquire any significant amount of mass prior to gas depletion. The detection of close-in Neptune-mass around M dwarf stars and the modest detection frequency of gas giants around solar-type stars are inconsistent with the results of series B in Figure 9a and therefore, we suggest that A_ν is substantially larger than unity.

An upper limit on the magnitude of A_ν may be inferred from models $x\text{C}$. With $A_\nu = 100$, the condition for the onset of migration becomes much more stringent and most cores do not have sufficient mass to undergo migration. For solar-type stars, a few relatively massive cores can form rapidly in disks with very large f_{d} . These systems can migrate to form close-in Jupiter-mass gas giants. The mass distribution of close-in planets around solar type stars (model 1.0C) is skewed to $10^3 M_\oplus$ with lower cut-off below $\sim 0.5 M_{\text{J}}$, which is inconsistent with the observed mass-period distribution of extra solar planets (Figure 1). For low-mass host stars (models 0.2C and 0.4C), many intermediate-mass planets can form during and after gas depletion. But they retain their initial semi major axis. The mass distribution of the close-in planets peaks near the mass of Saturn and hardly any planets have masses comparable to that of Neptune. These simulation results are again inconsistent with the observed mass-period distribution of extra solar planets. Furthermore, in series C, the deficit of planets with intermediate masses and periods is too pronounced to be consistent with observed one. Therefore, we infer $A_\nu \sim 10$.

6. Dependence on the disk mass

The expressions in equations (1) and (2) indicate that the growth rate and asymptotic mass of cores are increasing function of Σ_{d} . In the standard series of models, we set $h_{\text{d}} = (M_*/M_\odot)^2$. With this prescription, Σ_{d} of disks around low-mass stars is relatively small. Consequently, the emergence of gas giants occurs preferentially around massive stars.

The dependence of the disks' Σ_{d} on the M_* of their host stars is poorly known. On the theoretical side, gravitational instability may limit the amount of mass which can be retained by the disks, especially those around low-mass stars. But, smaller L_* 's and lower intensity of ionizing photons may also reduce the influence of the magneto-rotational instability (Gammie 1996) and the angular momentum transfer efficiency so that more mass may be stored in disks around low-mass stars. Best available observational data suggest $\dot{M} \propto M_*^2$ (see §2.2) but the dependence of Σ_{d} on M_* is poorly known. In view of these uncertainties, we introduce another two series of models.

The parameters of models $x\text{D}$ and $x\text{E}$ are identical to those of models x , respectively. The only difference is that we set $h_{\text{d}} = M_*/M_\odot$ in series D and it is set to be unity for all M_* in series E. In comparison with the standard models, disks around low-mass stars are less deficient in these new models while those around the solar type stars remain the same.

The predicted distributions for series D and E are shown in Figure 10. Since $M_{\text{p,mig}}$ and $M_{\text{p,trunc}}$

do not depend on Σ_d nor Σ_g , planets’ migration and gas accretion undergo the same paths as in standard models for the same mass planets. As a result, the mass distribution of close-in planets is self-similar among models x , xD , and xE . Since massive disks exist around lower mass stars more frequently in series D (and even more frequently in series E), the amplitude of mass distributions around lower mass stars are enhanced in these models. In series D and E, inferred frequency of Jupiter mass planets around M stars are comparable to those around G stars (Figure 10). The sparse detection of close-in Jupiter-mass and Neptune-mass planets around M stars suggests that the disk masses are rapidly increasing function of M_* as we have assumed in the standard models with $h_d = (M_*/M_\odot)^2$.

7. Summary and discussions

Observational discovery of extrasolar planets is advancing rapidly. We now have sufficient amount of data to carry out statistical characterization of planetary properties and to place constraints not only on the dominant mode of planet formation but also the range of physical quantities which determine their growth and migration rates. In this paper, we focused our discussion on the mass function of close-in planets around stars with various masses, in particular lower masses than the solar mass, because its origin is determined by the delicate balance of various processes and they are the most conspicuous companions of nearby stars. Although many ($\gtrsim 90\%$) planets which once migrated to the proximity of their host stars may be eliminated (Paper II), we can compare the mass distribution of close-in planets among around stars with various masses. If the elimination factor is taken into account, rough comparison is also possible between close-in and more distant planets.

Our results are summarized as follows.

1. Dynamically-isolated, close-in, Neptune-mass planets with silicate and iron cores can form in relatively massive disks around solar-type stars. But their frequency is expected to be an order of magnitude smaller than that of close-in Jupiter-mass planets.
2. Dynamically-isolated, close-in, Neptune-mass ice giants can form in lower-mass stars. Their frequency peaks around the M dwarfs. Since the luminosity of M dwarfs is weak, the ice boundary is located well inside 1 AU. These planets are formed at around 1AU but outside the ice boundary and their cores are primarily composed of volatile ices. Planets which migrated to the stellar proximity with masses in the range of $5 - 15M_\oplus$ may acquire, *in situ*, a limited amount of additional gas, but gas accretion is immediately quenched by gap formation because of small aspect ratio of the disk in the proximity of the host star. Because these planets compose mostly of icy material and M stars’ luminosity is relatively weak, they may have water-vapor atmosphere and water ocean (Léger et al. 2004).
3. Embryos with mass lower than $10M_\oplus$ cannot migrate to the proximity of their F, G, and

K dwarf host stars through type II migration. Detection of dynamically-isolated Earth-mass close-in planets may be attributed to type I migration of low-mass embryos (Ward 1997a), sweeping secular resonances (Lin et al. 2004), or sweeping mean motion resonances. Around late M dwarfs, however, dynamically-isolated, a few earth-mass planets can form with temperature comparable to that of the earth.

4. Around M dwarfs, the formation probability of gas giants is much reduced. The relatively low Σ_d prevents the emergence of sufficiently massive cores prior to the severe depletion of gas in their nascent disks, which is consistent with the results by Laughlin, Bodenheimer & Adams (2004).
5. The mass function of close-in planets generally have two peaks at about Neptune mass and at about Jupiter mass. The lower-mass peak takes the maximum frequency for M stars, while the higher-mass peak is much more pronounced around higher-mass stars (F, G, K dwarfs). These are because planets tend to undergo type II migration after fully accreting gas around the higher-mass stars while they tend to migrate faster than gas accretion around M stars. Unless the termination location of planetary migration is a decreasing function of M_* , close-in Neptune-mass planets around M dwarfs are easier to detect than those around G dwarfs.
6. The mass function of dynamically-isolated close-in planets around stars with various masses can also be used to calibrate the sufficient condition for the onset of planetary migration and for the termination of gas accretion due to planet-disk tidal interaction.

The metallicity dependence on frequency of extrasolar gas giant planets may not be easily accounted for by the gravitational instability scenario, e.g., (Boss 2001), while it is naturally accounted for by the sequential core accretion scenario that we are based on (Paper II). The condition of the gravitational instability is $1 > Q = c_s \Omega_K / \pi G \Sigma_g \propto M_*^{1/2} M_*^{1/2} / \Sigma_g = M_*^{1-\beta}$, and its radial wavelength $\lambda = 2\pi^2 G \Sigma_g / \Omega_K^2 \propto M_*^{\beta-1}$ (Toomre 1964) where $\Sigma_g \propto M_*^\beta$. Hence, the instability may be more limited and result in smaller clumps around lower-mass stars, which could account for the above features 4 and 5, if $\beta = 2$ is assumed as in the standard series in the present paper. However, if $\beta = 1$, the gravitational instability scenario cannot account for the above features 4 and 5, while the sequential core accretion scenario still shows the tendency for the features. More detailed study on the dependence of disk mass on stellar mass M_* is needed.

Our work is primarily motivated by the discovery of GJ436b (Butler et al. 2004). Our theoretical extrapolations can be tested with the following statistical properties of close-in planets to be discovered by various techniques.

1. As mentioned above, the mass function of dynamically-isolated close-in planets as a function of the spectral classes of their host stars is particularly useful in the determination of the growth, migration, and disk depletion time scales.

2. A comparison between the frequencies of gas giants with close-in orbits and those with extended orbits can provide constraints on the migration condition, survival criteria, and disk mass as functions of the host stars' mass.
3. In systems with multiple giant planets, the dynamical architecture may provide clues on whether the migration of the close-in planets are driven by planet-disk tidal interaction or sweeping secular resonance.
4. A comparison of atmospheric properties of close-in Neptune-mass planets around G dwarfs to that around M dwarfs can verify the conjecture that the former have silicate and iron cores whereas the latter have ice cores.

The following observations of protostellar disks may provide useful input to the model:

1. A spatially resolved image of disks can directly provide information of Σ_d and the temperature distribution around any given host star.
2. The dependence of Σ_d on the mass of the host stars determines the functional form of h_d .
3. A relation between the disk mass and accretion rate onto the host stars places a constraint on the rate of type II migration.
4. A direct measurement of the gas distribution is particularly important in determining τ_{dep} and h_g .

On the modeling side, we need to consider:

1. The possibility of radiative feedback on the termination of gas accretion.
2. The stoppage of type II migration and the survival of short-period planets.
3. The rate (and direction) of type I migration of cores.
4. The enhanced probability of multiple planet formation.
5. Effect of dynamical interaction between multiple planets during and after gas depletion.
6. The radial distributions of Σ_d and Σ_g . Effects of different power-law index of a dependence from -1.5 that we used. More realistic time evolution of Σ_g .
7. The influence of a stellar companion on the emergence and survival of planets.

Some of these issues will be addressed in future discussions.

We thank G. Laughlin, M. Nagasawa, G. Ogilvie, and S. Vogt for useful discussions, and the anonymous referee for useful comments. This work is supported by the NASA through NAGS5-11779 under its Origins program, JPL 1228184 under its SIM program, and NSF through AST-9987417 and by JSPS.

REFERENCES

- Aarseth, S. J., Lin, D. N. C., Palmer, P. L. 1993, *ApJ*, 403, 351
- Beckwith, S. V. W., & Sargent, A. I., 1996, *Nature*, 383, 139
- Balmforth, N. J. & Korycansky, D. G. 2001, *MNRAS*, 326, 833
- Bodenheimer, P., & Pollack, J. B. 1986, *Icarus*, 67, 391
- Bodenheimer, P., Hubickyj, O. & Lissauer, J. J. 2000, *Icarus*, 143, 2
- Boss, A. P. 2001, *ApJ*, 551, L167
- Boss, A. P., Wetherill, G. W. & Haghighipour, N., 2002, *Icarus*, 156, 291
- Bryden, G., Xingming, C., Lin, D. N. C., Nelson, R., & Papaloizou, J. C. B. 1999, *ApJ*, 514, 344
- Butler, P. et al. 2004, *ApJ*, in press
- D'Alessio, P., Calvet, N., Hartmann, L. 2001, *ApJ*, 553, 321
- Goldreich, P., & Tremaine, S. 1980, *ApJ*, 241, 425
- Greenberg, R., Hartmann, W. K., Chapman, C. R., & Wacker, J. F. 1978, *Icarus* 35, 1
- Gammie, C. F. 1996, *ApJ*, 457, 355
- Gu, P., Lin, D. N. C., & Bodenheimer, P. H. 2003, *ApJ*, 588, 509
- Haisch, K. E., Lada, E. A. & Lada, C. J. 2001, *ApJ*, 553, L153
- Hayashi, C. 1981, *Prog. Theor. Phys. Suppl.*, 70, 35
- Hayashi, C., Nakazawa, K. & Nakagawa, Y. 1985, *Protostars and Planets II*, ed. D. C. Black & M. S. Matthews (Tucson: Univ. of Arizona Press), 1100
- Ida, S., & Makino, J. 1993, *Icarus*, 106, 210
- Ida, S., Bryden, G., Lin, D. N. C. & Tanaka, H. 2000, *ApJ*, 534, 428
- Ida, S. & Lin, D. N. C. 2004, *ApJ*, 604, 388 (Paper I)
- Ida, S. & Lin, D. N. C. 2004, *ApJ*, 616, 567 (Paper II)
- Ikoma, M., Nakazawa, K. & Emori, E. 2000, *ApJ*, 537, 1013
- Ivanov, P. B., Papaloizou, J. C. B. & Polnarev, A. G. 1999, *MNRAS*, 307, 791
- Iwasaki, K., Emori, H., Nakazawa, K. & Tanaka, H. 2002, *PASJ*, 54, 471

- Kokubo, E. & Ida, S. 1996, *Icarus*, 123, 180
- . 1998, *Icarus*, 131, 171
- . 2000, *Icarus*, 143, 15
- . 2002, *ApJ*, 581, 666
- Koller, J., Li, H. & Lin, D. N. C. 2003, *ApJ*, 596, L91
- Kominami, J. & Ida, S. 2002, *Icarus*, 157, 43
- Laughlin, G., Steinacker, A. & Adams, F. C. 2004, *ApJ*, 608, 489
- Laughlin, G., Bodenheimer, P. & Adams, F. C. 2004, *ApJ*, 612, L73
- Léger et al. 2004, *Icarus*, 169, 499
- Lin, D. N. C. & Papaloizou, J. C. B. 1980, *MNRAS*, 191, 37
- Lin, D. N. C. & Papaloizou, J. C. B. 1985, *Protostars and Planets II*, ed. D. C. Black & M. S. Matthews (Tucson: Univ. of Arizona Press), 981
- Lin, D. N. C., & Papaloizou, J. C. B. 1993, in *Protostars and Planets III*, ed. E. H. Levy and J. I. Lunine (Tucson: Univ. of Arizona Press), 749
- Lin, D. N. C., Bodenheimer, P. & Richardson, D. 1996, *Nature*, 380, 606
- Lin, D. N. C., Nagasawa, M. & Thommes, E. W., submitted
- Lissauer, J. J. 1987, *Icarus*, 69, 249
- Lissauer, J. J. & Stewart, G. R. 1993
- Lubow, S. H., Seibert, M. & Artymowicz, P. 1999, *ApJ*, 526, 1001
- Marcy, G. W., Cochran, W. D., & Mayor, M. in *Protostars and Planets IV*, ed. V. Mannings, A. P. Boss and S. S. Russell (Tucson: Univ. of Arizona Press), 1285
- Malhotra, R. 1993, *Nature*, 365, 819
- Mayor, M. & Queloz, D. 1995, *Nature*, 378, 355
- McArthur, B. 2004, *ApJL*, 614, L81
- Mizuno, H. 1980, *Prog. Theor. Phys. Suppl.*, 64, 54
- Mohanty, S., Jayawardhana, R. & Navascués, 2003, *ApJ*, 593, L109
- Muzerolle, J. et al., 2003, *ApJ*, 592, 266

- Nagasawa, M., Tanaka, H. & Ida, S. 2000, *AJ*, 119, 1480
- Natta, A. et al., 2004, *A&A*, 424, 603
- Nelson, R. P., Papaloizou, J. C. B., Masset, F. & Kley, W. 2000, *MNRAS*, 318, 18
- Nelson, R. P. & Papaloizou, J. C. B. 2004, *MNRAS*, 350, 849
- Papaloizou, J. C. B. & Lin, D. N. C. 1995, *ARA&A*, 33, 505
- Pollack, J. B., Hollenbach, D., Beckwith, S., Simonelli, D. P., Roush, T., & Fong, W. 1994, *ApJ*, 421, 615
- Pollack, J. B., Hubickyj, O., Bodenheimer, P., Lissauer, J. J., Podolak, M., & Greenzweig, Y. 1996, *Icarus*, 124, 62
- Rafikov, R. R. 2003, *AJ*, 125, 922
- Sano, T. et al. 2000, *ApJ*, 543, 486
- Santos, N. et al. 2004, *A&A*, 426, L19
- Safronov, V. 1969, *Evolution of the Protoplanetary Cloud and Formation of the Earth and Planets* (Moscow: Nauka Press)
- Shakura, N. I. & Sunyaev, R. A. 1973, *A&A*, 24, 337
- Stevenson, D. J. 1982, *P&SS*, 30, 755
- Tanaka, H. & Ida, S. 1997, *Icarus*, 125, 302
- Tanaka, H., Himeno, Y., & Ida, S. 2004, submitted
- Thi, W. F., Blake, G. A., van Dishoeck, E. F., van Zadelhoff, G. J., Horn, J. M. M., Becklin, E. E., Mannings, V., Sargent, A. I., van den Ancker, M. E.; Natta, A. 2001, *Nature*, 409, 60
- Toomre, A. *ApJ*, 139, 1217
- Ward, W. 1981, *Icarus*, 47, 234
- Ward, W. 1986, *Icarus*, 67, 164
- Ward, W. 1997, *Icarus*, 126, 261
- Ward, W. 1997, *ApJ*, 482, L211
- Wetherill, G. W. 1980, *ARAA*, 77, 330
- Wetherill, G. W. & Stewart, G. R. 1989, *Icarus*, 77, 330

- Wuchterl, G., Guillot, T. & Lissauer, J. J. 2000, Protostars and Planets II, ed. V. Mannings, A. P. Boss & S. S. Russell (Tuscon: Univ. of Arizona Press), 1081
- Wyatt, M. C. et al. 2003, MNRAS, 342, 876

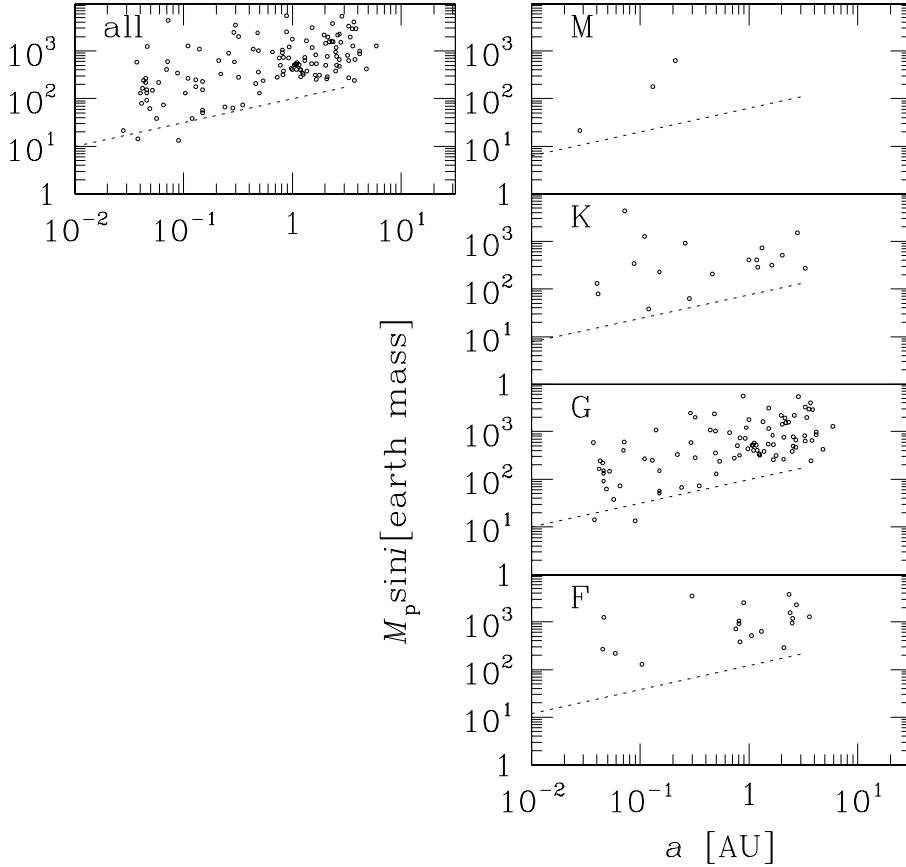


Fig. 1.— The distributions of semimajor axis (a) and mass ($M_p \sin i$) of discovered extrasolar planets. Unit of mass is Earth mass M_\oplus (Jupiter mass is $M_J \simeq 320M_\oplus$). The data are taken from “The Extrasolar Planets Encyclopedia” (<http://cfa-www.harvard.edu/planets/>) as of February, 2005. The planets around subgiants and those discovered by transit survey are excluded. The right panels show the planets around M, K, G, and F stars, respectively. The left panel shows all the data. The dotted lines show observational limits ($v_r = 10$ m/s) for doppler survey. Detection of larger a ($\gtrsim 3$ AU) planets, which have longer orbital periods, is also limited.

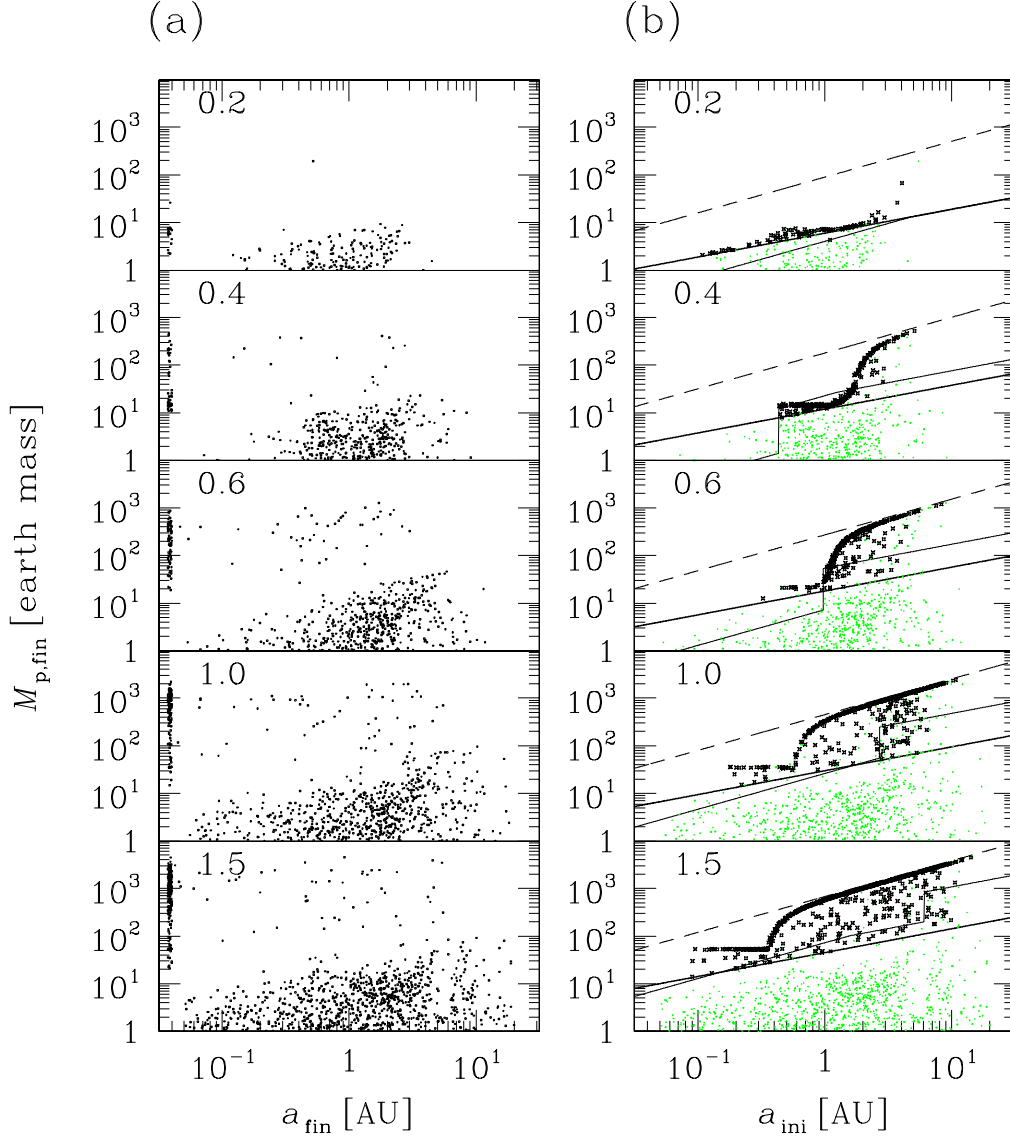


Fig. 2.— The distributions of semimajor axis (a) and mass (M_p) of planets predicted by the Monte Carlo simulations. (a) final semimajor axes (a_{fin}) and masses ($M_{p,\text{fin}}$) at $t = 10^9$ yrs, and (b) initial semimajor axes (a_{ini}) and $M_{p,\text{fin}}$. The symbols x ($= 0.2, 0.4, 0.6, 1.0$ and 1.5) represent the host star mass scaled by the solar mass, M_*/M_\odot . In (b), close-in planets with $a_{\text{fin}} < 0.05\text{AU}$ are marked by black crosses, while the other planets are marked by gray dots. The thin solid black lines indicate the isolation mass $M_{c,\text{iso}}$ with $f_d = 30$. The thick solid black lines express the critical mass for radial migration, $M_{p,\text{mig}} = A_\nu M_{g,\text{vis}}$ with $A_\nu = 10$. The dashed lines are the truncation mass for gas accretion, $M_{p,\text{trunc}} = A_{\text{th}} M_{g,\text{th}}$ with $A_{\text{th}} = 3.4$.

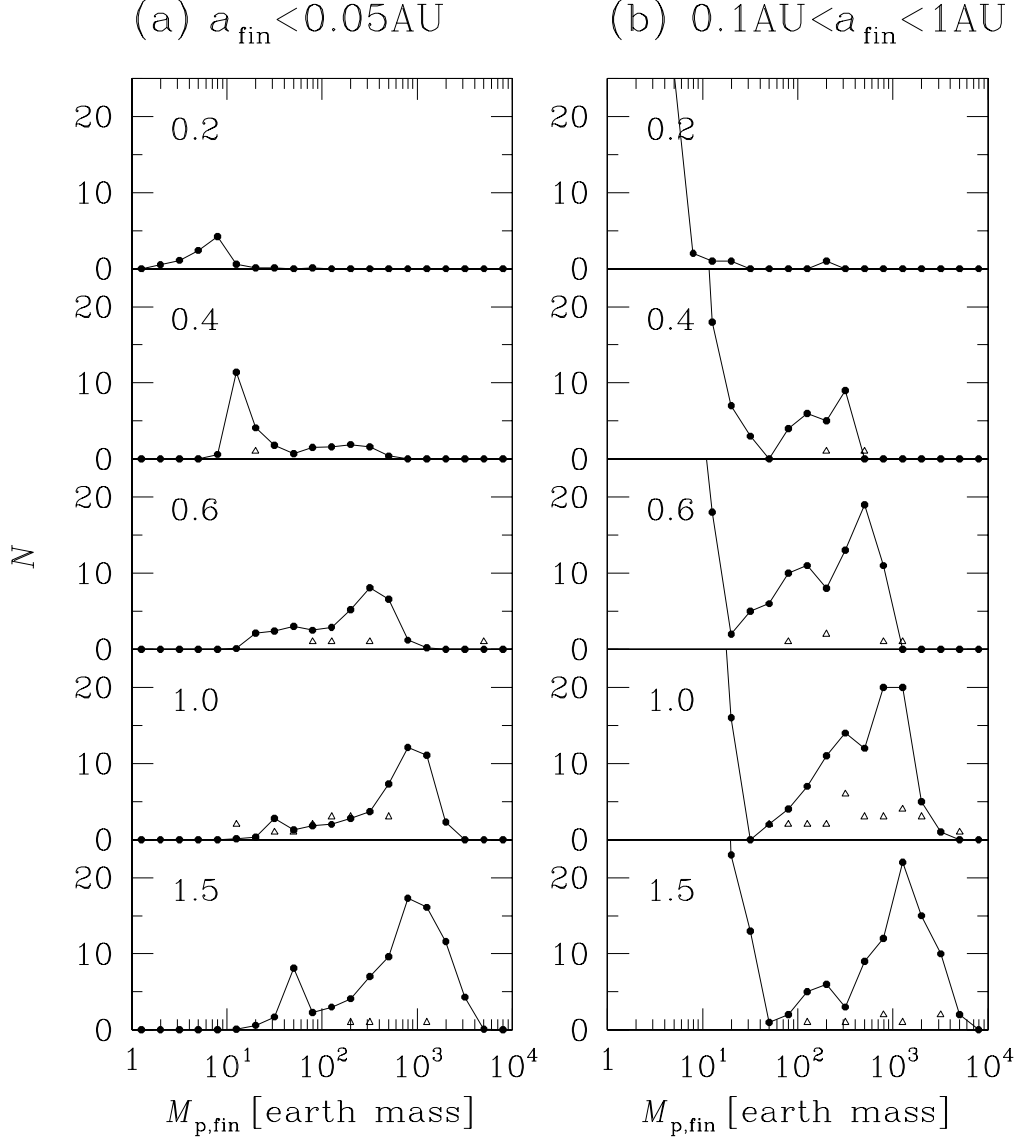


Fig. 3.— The calculated distribution of final mass of planets for (a) close-in planets at $a_{\text{fin}} < 0.05\text{AU}$ and (b) planets at $0.1\text{AU} < a_{\text{fin}} < 1\text{AU}$ (filled circles). The labels x are the same as Figure 2. Since it is expected that most of close-in planets may fall onto their host stars, the calculated amplitude N in (a) is reduced by a factor 10. Observed distributions are also plotted with open triangles. The $\sin i$ factor is neglected for simplicity (it enhances the observed values only by $4/\pi$ on average). The number of runs in each model does not reflect the number of targets for current doppler survey. Also note that observed distributions do not exactly correspond to host stars’ mass of each model.

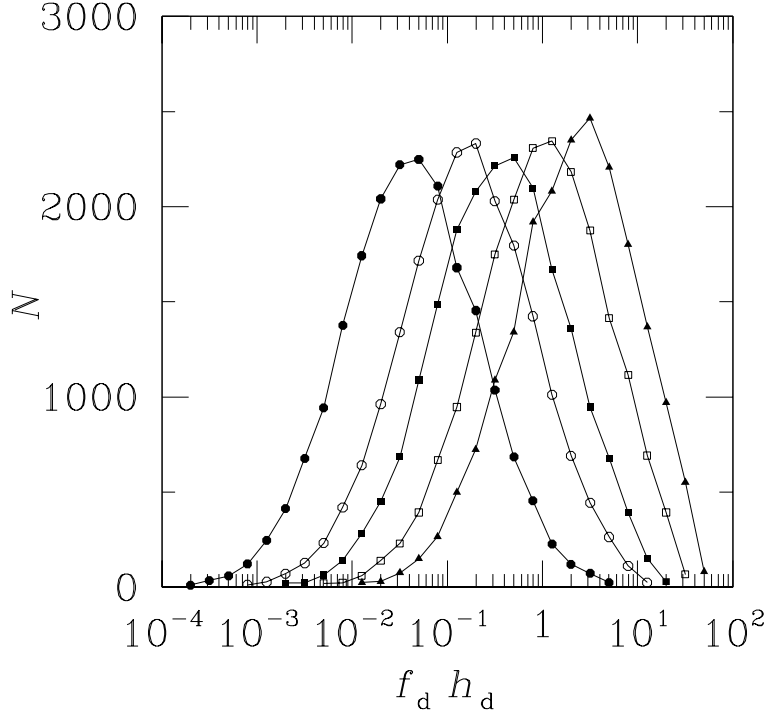


Fig. 4.— The $f_d h_d$ distribution we used for the standard model, which is a gaussian distribution in terms of $\log_{10} f_d$ with a center at $\log_{10} f_d = 0$ and dispersion of 1. In the standard model, we assume $h_d \propto (M_*/M_\odot)^2$. We omit the high $h_d f_d$ tail at $> 30(M_*/M_\odot)$, since such heavy disks are self gravitationally unstable. Filled circles, open circles, filled squares, open squares and filled triangles represent the cases of $M_* = 0.2, 0.4, 0.6, 1.0$, and $1.5M_\odot$.

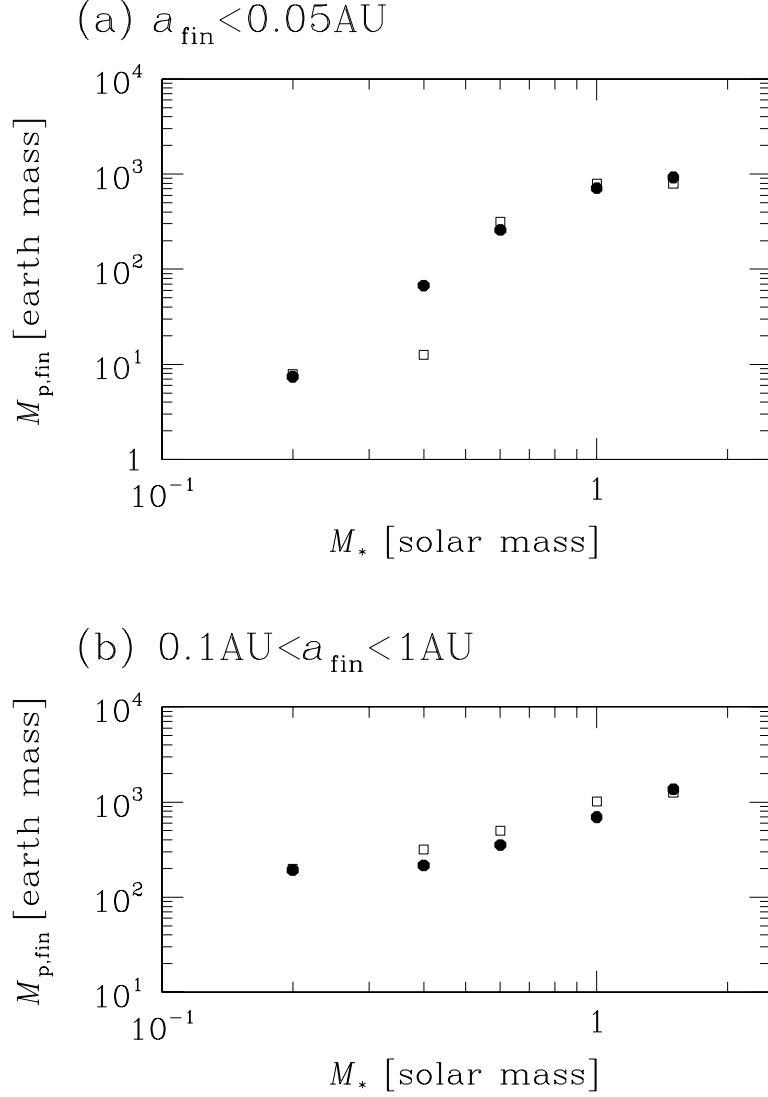


Fig. 5.— The mean mass and the characteristic mass associated with the peak of the mass distribution given in Figures 3, as a function of host stars’ mass M_* . (a) the close-in planets with $a_{\text{fin}} < 0.05 \text{ AU}$ and (b) the planets at $0.1 \text{ AU} < a_{\text{fin}} < 1 \text{ AU}$. The mean mass and the peak mass are plotted with filled circles and open squares. For (b), only planets with M_{p} over a deficit ($M_{\text{p}} > 50 M_{\oplus}$) are considered (see Figures 2a and 3b).

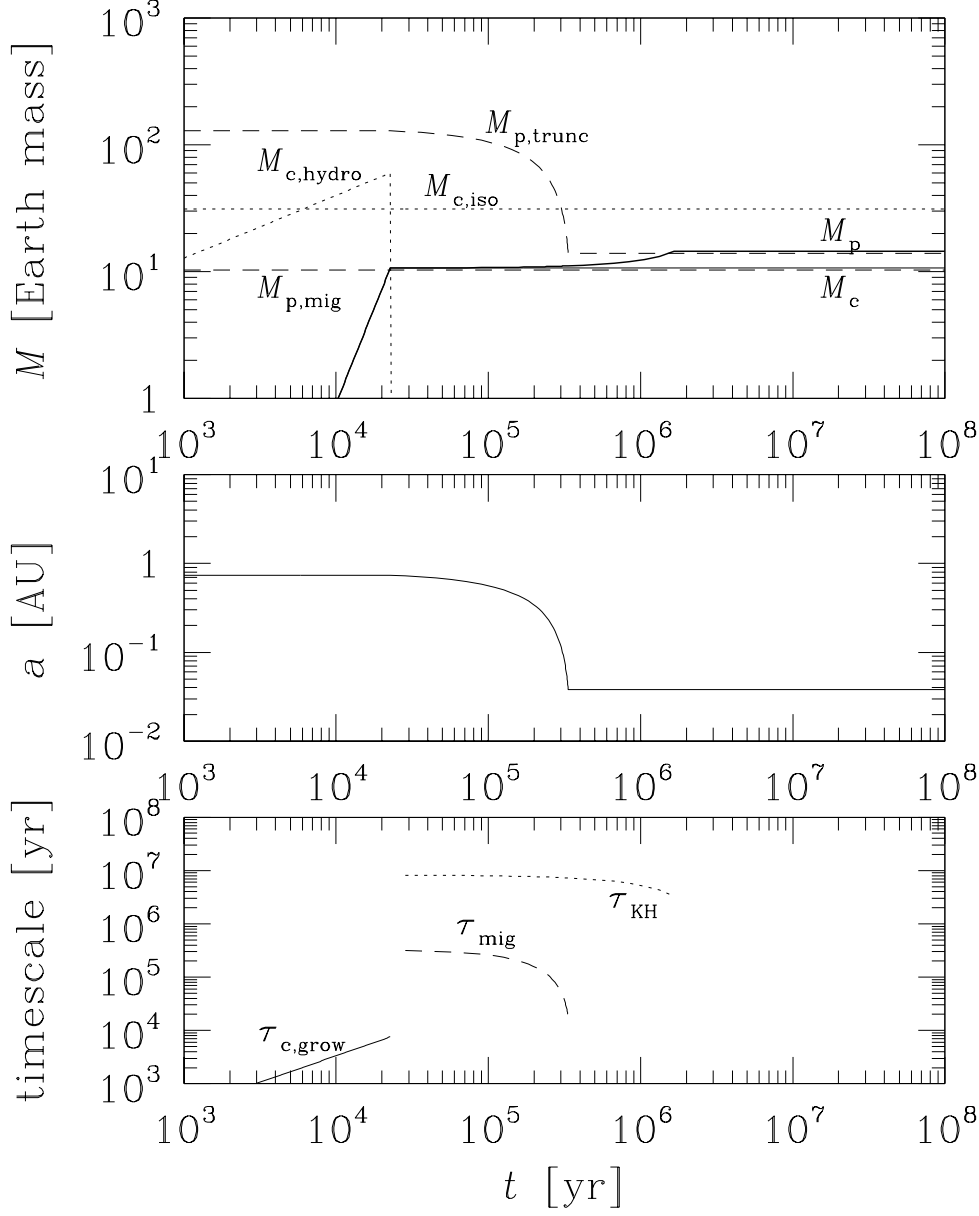


Fig. 6.— An example of formation of a close-in Neptune-mass planet around an M star. A planet is initially at 0.74 AU in a disk with $f_d h_d = 7.2$ and $\tau_{\text{dep}} = 9.2$ Myr around a star with $M_* = 0.4 M_\odot$. The upper and middle panels show time evolution of mass and semimajor axis of the planet. In the upper panel, the isolation mass of a core ($M_{c,\text{iso}}$), its critical mass for initiation of gas accretion ($M_{c,\text{hydro}}$), the planet’s critical mass for migration ($M_{g,\text{mig}}$) and the truncation mass of gas accretion ($M_{g,\text{trunc}}$) are plotted for comparison. In the lower panel, core accretion time scale ($\tau_{c,\text{grow}} = M_c / \dot{M}_c$), gas accretion time scale (τ_{KH}) and migration time scale (τ_{mig}) are plotted.

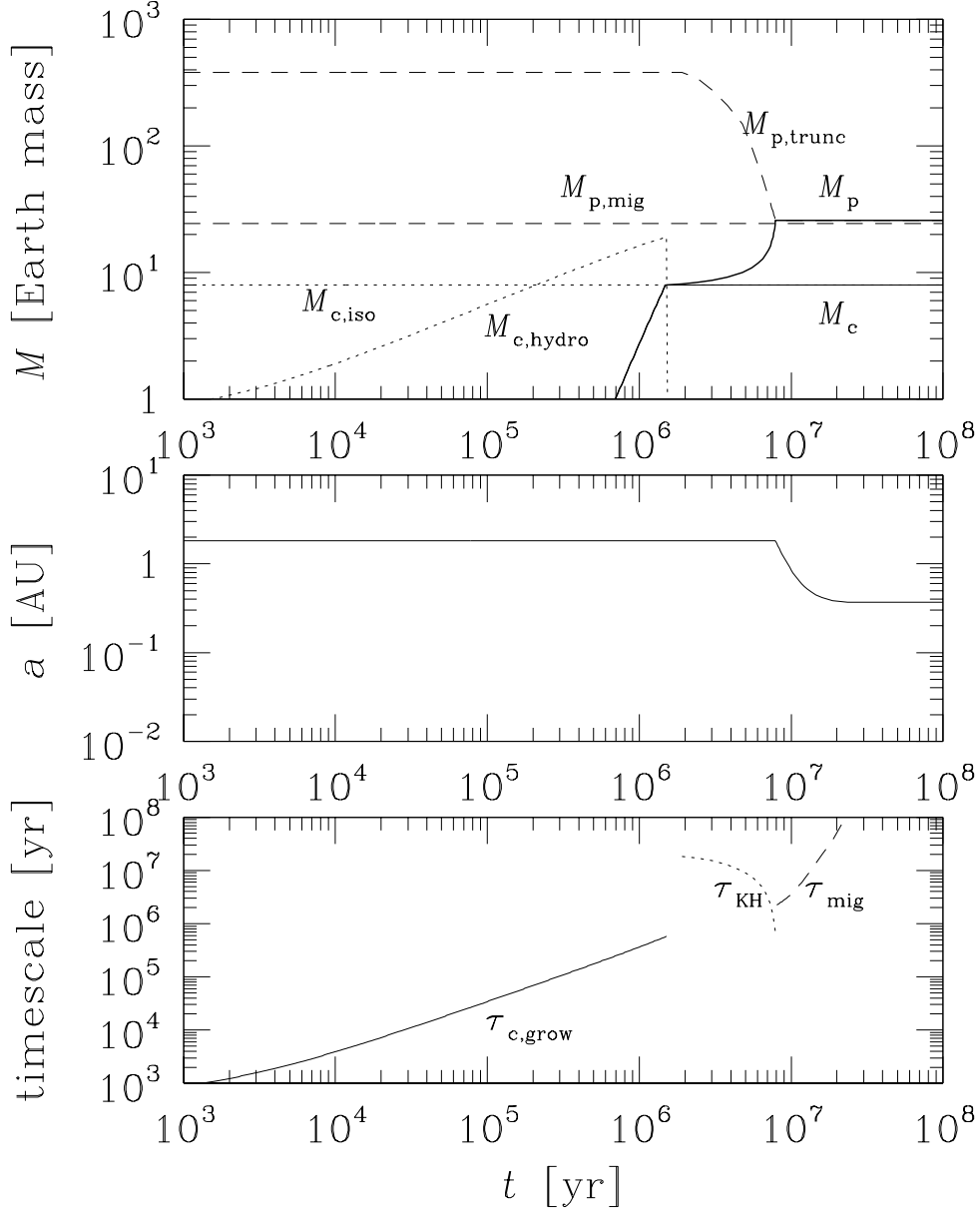


Fig. 7.— An example of formation of an intermediate-mass planet with intermediate period around a K star. A planet is initially at 1.8AU in a disk with $f_d h_d = 2.0$ and $\tau_{dep} = 2.3$ Myr around a star with $M_* = 0.6M_\odot$. Notations are the same as Figure 5.

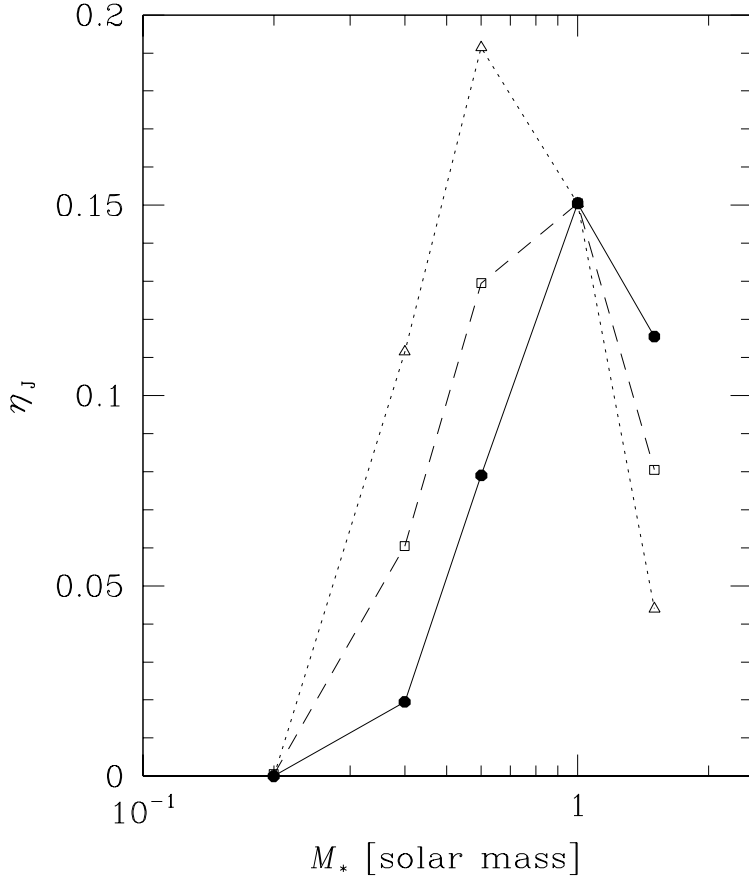


Fig. 8.— The theoretically predicted fraction (η_J) of stars which bears giant planets currently detectable with current doppler survey, as a function of their mass (M_*). The results of the standard model with $h_d = (M_*/M_\odot)^2$ are plotted by filled circles, while the results of series D and E with $h_d = M_*/M_\odot$ and 1 are plotted by open squares and triangles, respectively. The detectable conditions are radial velocity $v_r > 10\text{m/s}$ and period $P < 4$ years. We do not include planets stalled at 0.04AU in the evaluation of η_J , since most of them may fall onto their host stars. The distribution of f_d is the same as in Figure 4. For each f_d , a is selected as $\log(a_{j+1}/a_j) = 0.2$ ($j = 1, 2, \dots$).

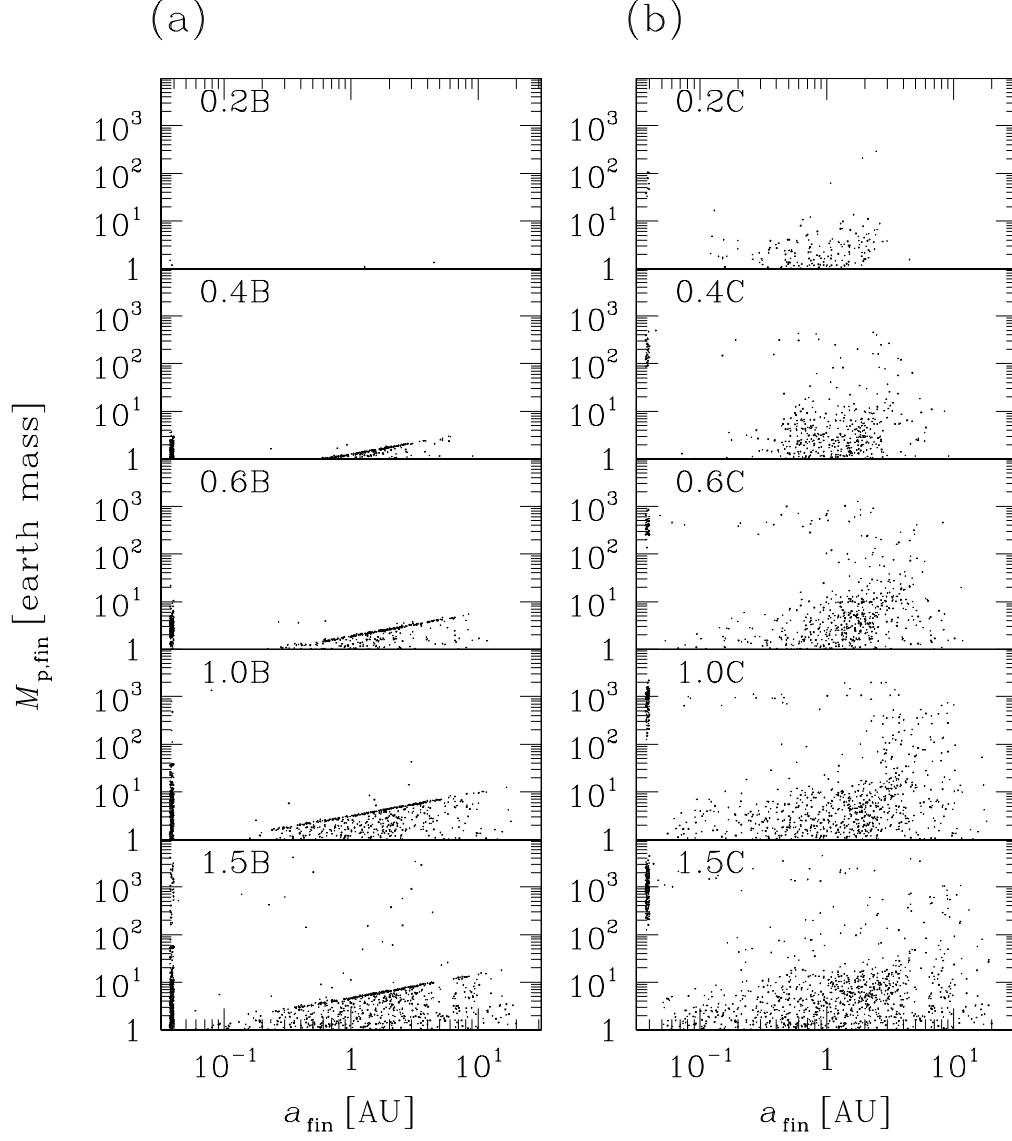


Fig. 9.— The predicted distributions of semimajor axis (a) and mass (M_p) of planets in the final state at $t = 10^9$ yrs: (a) model x B with $M_{p,\text{mig}} = M_{g,\text{vis}}$, (b) model x C with $M_{p,\text{mig}} = 100M_{g,\text{vis}}$, where x in x B and x C represent the results with $M_* = xM_\odot$.

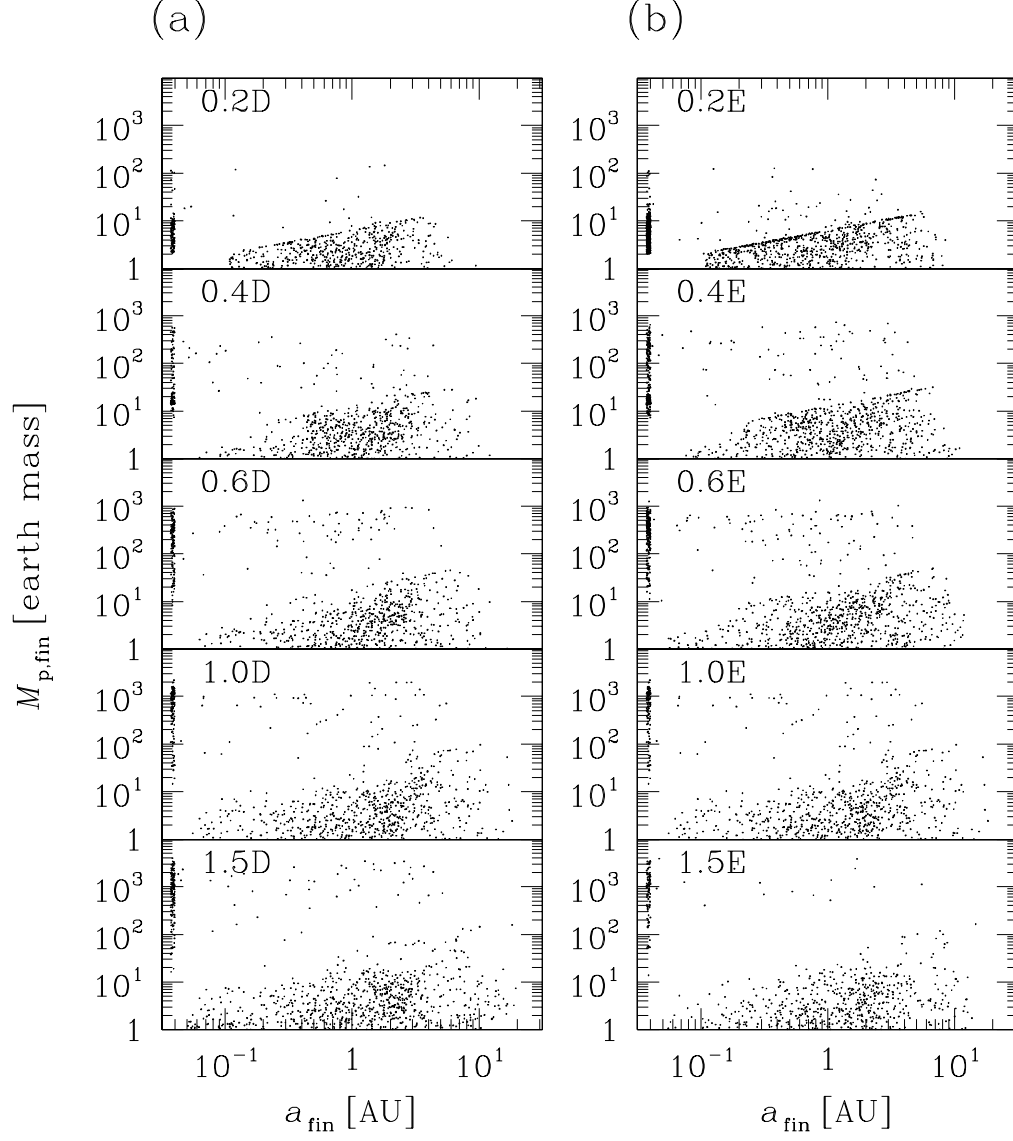


Fig. 10.— The same as Figure 9 except (a) model x D with $h_d = M_*/M_\odot$, (b) model x E with $h_d = 1$.